
NOVEL 3D SCENE UNDERSTANDING APPLICATIONS FROM RECURRENCE IN A SINGLE IMAGE

Shimian Zhang^{1,*}, Skanda Bharadwaj^{1,*}, Keaton Kraiger^{1,*}, Yashasvi Asthana^{2,†}, Hong Zhang^{3,†}, Robert Collins¹, and Yanxi Liu¹

¹Pennsylvania State University, PA, US

²Nimble Robotics Inc., CA, US

³Meituan AI., Beijing, China

¹{svz5303, ssb248, kbk5531, rtc12, yu111}@psu.edu

²yashasvi@nimble.ai

³zhanghong50@meituan.com

ABSTRACT

We demonstrate the utility of recurring pattern discovery from a single image for spatial understanding of a 3D scene in terms of (1) vanishing point detection, (2) hypothesizing 3D translation symmetry and (3) counting the number of RP instances in the image. Furthermore, we illustrate the feasibility of leveraging RP discovery output to form a more precise, quantitative text description of the scene. Our quantitative evaluations on a new 1K+ Recurring Pattern (RP) benchmark with diverse variations show that visual perception of recurrence from one single view leads to scene understanding outcomes that are as good as or better than existing supervised methods and/or unsupervised methods that use millions of images.

1 Introduction

Pattern discovery from 2D images is fundamental for humans and robots to understand the 3D world [1, 2, 3, 4], in particular **Recurring Patterns (RP)**, referring to the broadly defined a set of “*things that recur*” [5]. The non-identical (both geometrically and photometrically) yet similar elements comprising an RP are named **RP instances** (Fig. 1). Different from the term “object” widely used in the literature, an RP instance may or may not correspond to an object completely (Fig. 1a, 1c, 1d), yet we show in this work that RP instances discovered in an unsupervised manner can lead to novel applications in 3D scene understanding. Our working hypothesis is that the recurrence of class-agnostic things (a much more relaxed notion than symmetry [6, 7]) may imply semantic significance in a way similar to how humans perceive/discover new environments class-agnostically [8].

Unsupervised Recurring Pattern Discovery (URPD) is a challenging class-agnostic, zero-shot task. Relevant to scene understanding, recurrence can be leveraged to infer aspects of 3D scene geometry. RP instances of similar size in 3D viewed under perspective projection appear differently-sized in 2D, allowing estimation of relative depths. RP patterns frequently consist of colinear instances in 3D, and these project to 2D instances leading to a vanishing point, from which the 3D orientation of the line of instances can be inferred with respect to the camera view [9, 10]. Furthermore, colinear RP instances are often equally spaced in 3D, and this *3D translation symmetry* [11] can be quantitatively evaluated and hypothesized in 2D using by projective invariants measures. URPD from a single view can lead to a general approach for single view metrology [12, 13], leveraging class-agnostic RP discovery rather than needing explicit line detection [12] or known-class (e.g. pedestrian) detection [13].

Previous work on URPD [5] had limited success due to a lack of computational feasibility, generality and benchmarking, and missed the opportunity to infer 3D scene geometry from observations of recurrence. Our main contributions in this work include:

*The authors contribute equally to this paper.

†The work is accomplished at The Pennsylvania State University.

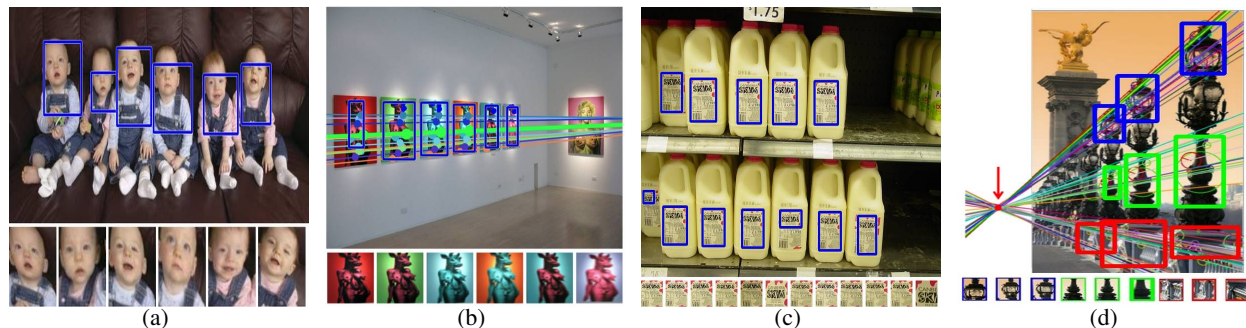


Figure 1: RP examples: (a) six similar baby faces, (b) six similar paintings, vanishing point (VP) detected (outside of the image), potential 3D translation symmetry discovered, (c) 12 milk labels, (d) three distinct RPs captured from different regions of the lamps, with a VP found (outside of the image). These examples show that an RP instance does not necessarily correspond to an object: an RP is simply a set of similar visual entities that recur within an image.

- We introduce an RP-benchmark dataset of 1K+ images collected across diverse sources, labeled with RPs and RP-instances (Sec. 4.1), including a benchmark subset of 147 images with labeled ground truth vanishing points.
- We re-implement an enhanced version of [5] by a new two-stage **RE**currence for **SC**ene **U**nderstanding (RESCU) architecture, with an unsupervised stage-I (Sec. 3.1) followed by a self-supervised stage-II (Sec. 3.2). Both stages outperform the baseline method [5] on our 1K+ RP benchmark image set (Sec. 4.2).
- We introduce three novel downstream URPD applications for 3D scene understanding:
 1. Vanishing Point Detection (VPD) without straight line requirements (Sec. 5.1);
 2. 3D translation symmetry prediction (Sec. 5.2);
 3. RP instance counting (Sec. 5.3).

These are quantitatively evaluated and compared with existing methods. In addition, we qualitatively illustrate how the three downstream URPD outcomes on scene understanding can enhance image captioning (Sec. 5.4) to achieve a more precise geometric and quantitative scene understanding from a single image.

2 Related Work

2.1 Recurring Pattern vs. Object Discovery

Recurring pattern discovery (RPD) is commonly compared with co-recognition / segmentation of objects [15, 19, 21], unsupervised object discovery [37, 38] and object co-localization [29, 39]. RPD is different from these object based approaches, which aim at localizing objects of the same known category co-occurring across multiple images. RPD adapts a broader definition of co-occurring instances that are not necessarily complete objects, and can find recurring instances from a single image. Many co-localization methods [29, 39] require a collection of unlabeled or semi-labeled images seen for common object discovery, while RPD is a zero-shot method. RPD is also different from repeated pattern detection approaches [31, 32, 33], which aims at detecting the pattern that are periodically repeated without any distortion. RPD aims at finding recurrence in a more relaxed notion than symmetry.

Table 1: Comparison of recurring pattern discovery approaches.

Approach	Matching Strategy	Unsupervised	Partial Matching	#Input images	Output
[14, 15, 16, 17]	Pairwise-Object	Yes	N/A	= 2	2 Objects
[18, 19, 7]	Pairwise-Object	Yes	N/A	≤ 2	2 Objects
[20, 14, 21]	Pairwise-Object	Yes	Yes	≥ 1	2 – 10 Objects
[22]	Pairwise-Visual Word	Yes	No	≥ 1	≥ 1 RPs
[23, 24, 25, 26, 27, 28]	Cross-Image	Yes	Yes	>> 2	N/A
[29, 30]	Cross-Image	Yes	N/A	>> 2	≥ 1 Objects
[31, 32, 33]	Pairwise-Visual Word	Yes	No	= 1	≥ 2 RP instances
[34]	Pairwise-Visual Word& Instance	No	Yes	= 1	= 1 RP
[35]	Co-occurrence Features	No	N/A	>> 2	= 1 Object
[36]	Query Image & Exemplars	No	Yes	= 1	≥ 2 RP instances
(Ours) RESCU	Pairwise-Visual Word & Instance	Yes	Yes	= 1	≥ 1 RPs

Tab. 1 shows a summary and comparison of different methods in terms of input/output and matching strategy. From Tab. 1, [5] and our approach are the only methods that discover class agnostic recurring pattern from a single image in an unsupervised fashion. Thus we treat [5] as our baseline. However, for RP instance counting evaluation, we also compare with [34] on the same dataset. It should be pointed out that [34] requires a given localization of *logo* regions in grocery product detection scenario (equivalent to giving an RP instance as input) before the RP discovery.

Our URPD method differs from all the existing methods in that we have no pre-assumption on the types of RPs to be found, except *something in the image recurs*. We experiment with both hand-crafted features (i.e., SIFT in stage-I) and deep features (i.e., CNN activations in stage-II), with a set of effective search strategies. Our stage-II is different from self-supervised approaches like [40, 41, 42], which propose various pretext tasks to generate pseudo labels automatically from the pretext tasks including image puzzling [40], inpainting [42], etc. In stage-II, we obtain generated RPs from stage-I as pseudo labels, to self-train a model to search for more RP-instances.

2.2 Recurring Pattern vs. Object/Instance Dataset

Most existing datasets are not suitable for URPD evaluation because they either fail to group instances based on visual similarity or lack of variety. Widely used object detection datasets [43, 44] have instance-level annotations categorized by object class, like person, cats, bottles, but do not label instances by visual similarity. Datasets like [45, 46] are designed for object detection in the specific domains of grocery product and car counting, respectively, and thus lack variety. The data in [47] contains both semantic and instance-wise annotations, and semantic instances belonging to the same class can be viewed as RP instances in many cases. However, the dataset is limited to city street-view images.

We introduce a new benchmark dataset of $1K+$ images (RP-1K) collected from a wide range of sources and viewpoints. Each image is manually labeled as containing single/multiple RPs. For each RP, the multiple RP instances are labeled with bounding boxes or finer-grained contours (Sec. 4.1).

2.3 Scene Understanding

3D scene understanding, briefly summarized in Table 2, has made substantial progress in the recent years. But little work has been done in trying to understand a 3D scene in the context of certain fundamental aspects such as vanishing point and repeating patterns that can be used as powerful tools to understand the geometry of the 3D scene. Our method is significantly different from the aforementioned methods in that we try to infer the 3D scene aspects by merely using the RPs to detect vanishing points and predicting translation symmetry in the 3D scene from a single image.

Table 2: Summary of 3D Scene Understanding Methodologies.

Literature	Applications
[48, 49, 50]	Performs depth estimation in the context of scene understanding.
[51, 52]	Dense captioning involving object-level 3D scene understanding.
[53, 54]	Performs Semantic Segmentation for visual scene understanding.
(Ours) RESCU	Prediction of Vanishing point, inferring existence of translation symmetry, counting RP-instance and enhancing scene captioning.

2.3.1 Vanishing Point Detection

Several algorithms have been developed to find vanishing points (VPs) from a single image [55, 56, 57, 58], which are heavily dependent on explicit line segments. Recently, [58] present a network based on a novel *conic convolution* operator that efficiently evaluates support across the image for hypothesized VP directions sampled on the Gaussian sphere, yet support is still based on strength of the response of learned edge filters oriented locally towards the VP. However, in real-world images, straight line or edge evidence may not always be explicit: e.g. Fig. 1d where lines leading to a VP are implicit. In this paper, we attempt to detect and quantitatively validate VPs by discovering these *implicit* lines using feature correspondences among RPs.

2.3.2 Translation Symmetry Detection

RP instances that are co-linear frequently also exhibit *translation symmetry*, meaning adjacent pairs of instances have equal distance between them along a line in 3D. Translation symmetry has been used as a constraint for perceptual grouping [10] and to recover 3D structure [59]. RPs with translation symmetry in 3D space maintain a mathematical relationship with their corresponding 2D image projections, defined by the cross-ratio [9]. Once they are discovered, these RPs can be rectified to remove perspective foreshortening, revealing a simpler, “frontal” appearance.

2.3.3 Counting Problem

RPD can benefit scene understanding by using number of detected RP instances to estimate the count of recurring instances in an image (e.g., grocery product counting [34]). Typical supervised object counting approaches [60, 61] may not perform well in unseen scenes. Class-agnostic and few-shot methods [62, 63, 64, 36, 65] often rely on references as input or are limited to single-class counting. Our method is able to discover and count multiple unseen RP instances and does not require any additional input.

Repetition counting in video domain [66, 67] is typically a class-agnostic task, where the repetitive activity can be any movement happened in real world. Repetition counting can be viewed as RP instance counting in spatial-temporal domain. In this paper, we focus on the application of RP discovery from 2D images and enhance a better understanding of 3D scene.

2.4 Image Captioning

Image captioning is a long standing task in computer vision which can provide a semantic understanding for a given image [68]. Commonly, efforts in deep learning-based image captioning have used pre-trained object detection networks [69] to identify salient image regions to caption [70]. Additionally, visual question answering (VQA) is a well explored research area in computer vision and natural language processing. VQA systems strive to correctly answer natural language questions about a given image. Recent work in unified vision-language models has demonstrated state-of-the-art results in both image captioning and VQA tasks through exploiting learned features from both visual and language modalities [71, 72, 73]. Despite these advances, current datasets frequently used in image captioning and VQA pre-training such as COCO do not contain a large number of RP instances we are interested in. Thus, we propose utilizing our discovered RP information from images to both enhance image captions and create new image-caption pairs with existing of-the-shelf models.

3 Methodology

Fig. 2 illustrates our overall approach with an image example. There are two major stages of Unsupervised Recurring Pattern Discovery (URDP): Stage-I performs initial, multi-threaded detection of one or more RPs, and Stage-II uses RP instances found in Stage-I to train a CNN classifier to extend each RP by finding additional RP instances. Final RPs output from Stage-II are then used in three downstream vision tasks: 1) vanishing point detection, 2) translation symmetry detection, 3) RP instance counting. The outputs of downstream tasks ultimately enhance image captioning for a better 3D scene understanding.

3.1 RESCU Stage-I: Multiple RP Discovery

3.1.1 Recurring Pattern Discovery

Similar to [5], we denote a *recurring pattern* mathematically as a $M \times N$ matrix Ω , where each row corresponds to a distinct *visual word* and each column corresponds to a distinct *RP instance* (Fig. 3a). We define each 2×2 sub-matrix $\Omega_{2,2}$, formed by choosing 2 rows m_1, m_2 and 2 columns n_1, n_2 of Ω as a *Unit Recurring Pattern* (URP). A URP is the smallest recurring pattern (Fig. 3b). The affinity score u of a URP $\Omega_{2,2}$ is measured by

$$u(m_1, m_2, n_1, n_2 | \Omega) = \exp(-\Delta_s^2 - \Delta_\theta^2) \quad (1)$$

where Δ_s and Δ_θ measure normalized scale and angular differences, defined as follows:

Following [5], we first define URP instance size ratio $r = \frac{d(f_{11}-f_{21})}{d(f_{12}-f_{22})}$, where $d(\cdot)$ is the Euclidean distance between two features of an URP instance.

We then define $D_s(f_i, f_j)$ as the normalized scale difference by RPI size ratio r of two SIFT features f_i and f_j , as follows:

$$D_s(f_i, f_j) = \frac{s_i - r \cdot s_j}{s_i + r \cdot s_j} \quad (2)$$

where s_k is the scale of feature f_k .

Similarly, we define $D_\theta(f_i, f_j)$ as the normalized angle difference by RPI size ratio r of two SIFT features f_i and f_j , as follows:

$$D_\theta(f_i, f_j) = \frac{\theta_1 - r \cdot \theta_2}{\theta_1 + r \cdot \theta_2} \quad (3)$$

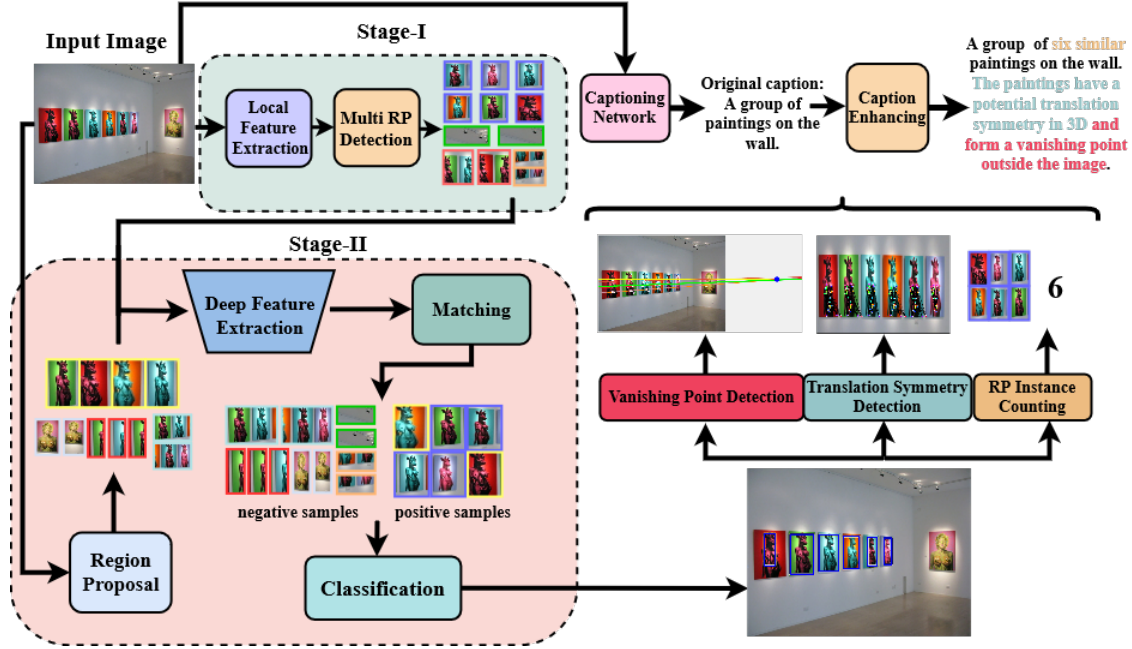


Figure 2: **Overview of our proposed two-stage method.** RESCU is comprised of two primary stages. **Stage-I.** We extract features from the image to perform unsupervised RP detection and obtain a set of candidate RP(s) and their corresponding region proposals. **Stage-II.** Candidate RP image crops discovered in Stage-I are passed through a frozen pre-trained feature extractor to obtain their corresponding feature representations. Region proposals derived from the original image are sent through the same extractor to obtain a second set of representations. We apply clustering to the features obtained from the region proposals and RP crops to perform matching and ultimately derive sets of positive and negative samples to train the final RP classifier. The predicted RP(s) are then used in **three downstream tasks**: RP instance counting, vanishing point detection, and translation detection. We show the discovered information may be used to enhance image captions.

Finally, we define Δ_s as the largest normalized scale difference:

$$\Delta_s = \max(D_s(f_{11}, f_{12}), D_s(f_{21}, f_{22})) \quad (4)$$

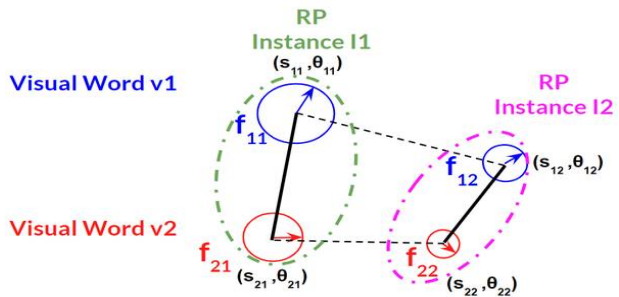
We define Δ_θ as the largest normalized angle difference:

$$\Delta_\theta = \max(D_\theta(f_{11}, f_{12}), D_\theta(f_{21}, f_{22})) \quad (5)$$

Unsupervised recurring pattern discovery (URPD) becomes an optimization problem for $\Omega^* = \arg \max_{\Omega, M, N} \{U(\Omega_{M, N})\}$ where

	RP-I ₁	RP-I ₂	...	RP-I _q
VW ₁	f_{11}	f_{12}	...	f_{1q}
VW ₂	f_{21}	f_{22}	...	f_{2q}
...
VW _p	f_{p1}	f_{p2}	...	f_{pq}

(a) an RP Matrix



(b) Unit Recurring Pattern (URP)

Figure 3: (a) an RP matrix, rows are features belonging to the same visual word, and columns are features belonging to the same RP instance. (b) a Unit Recurring Pattern (URP) is formed from the RP matrix by choosing two visual words (rows) and two RP instances (columns) to select four visual primitives, e.g. local SIFT features, $(f_{11}, f_{12}, f_{21}, f_{22})$, each of which has a scale s and angle θ .

$$U(\Omega_{M,N}) = \frac{1}{M \cdot N} \sum_{\substack{m_1, m_2=1..M \\ n_1, n_2=1..N}} u(m_1, m_2, n_1, n_2 | \Omega). \quad (6)$$

3.1.2 URP-based Search

To optimize Eq. 6, the baseline approach [5] adopts the GRASP [74] optimization with randomly selected 2 visual words as initial. For robustness on various types of images, more initials can benefit the approach on discovering RPs. However, [5] is lack of scalability to multiple initials due to computation expense which leads to a prolonged searching time.

We propose a URP-based approach to improve the robustness and scalability of [5] as follows: In each detection iteration, our approach maintains an RP matrix for each initial as Fig. 3a shows. The algorithm expend the URP (as a 2×2 initial matrix) with two movement directions: (1) add/remove a column, (2) add/remove a row.

Without losing generalizability, consider the current RP as $\Omega_{p,q}$ with p visual words, q RP instances as Fig 3a shows. To add a column for one more instance is to add a series of features $\{f_{1,q+1}, f_{2,q+1}, \dots, f_{p,q+1}\}$ into column $(q + 1)$, to form RP $\Omega_{p,q+1}$. To find the candidate feature $f_{i,q+1}$ to be put to visual word i , we define the visual word affinity sum-up score of $f_{i,q+1}$ respect to $\Omega_{p,q+1}$, as follows:

$$\mathbf{V}(f_{i,q+1} | \Omega_{p,q+1}) = \sum_{j \in [1,q]} V(f_{i,q+1}, f_{i,j}) \quad (7)$$

$$V(f_{i,q+1}, f_{i,j}) = \sum_{\substack{k \in [1,p], \\ k \neq i}} u(f_{i,q+1}, f_{i,j}, f_{k,q+1}, f_{k,j}) \quad (8)$$

$$(9)$$

hence,

$$\mathbf{V}(f_{i,q+1} | \Omega_{p,q+1}) = \sum_{j \in [1,q]} \sum_{\substack{k \in [1,p], \\ k \neq i}} u(f_{i,q+1}, f_{i,j}, f_{k,q+1}, f_{k,j}) \quad (10)$$

$\mathbf{V}(f_{i,q+1} | \Omega_{p,q+1})$ measures the overall affinity of URPs containing $f_{i,q+1}$ in $\Omega_{p,q+1}$. A candidate feature $f_{i,q+1}$ that maximize $\mathbf{V}(f_{i,q+1} | \Omega_{p,q+1})$ will be added to row i , column $q + 1$ of RP $\Omega_{p,q+1}$. Similarly column-wise.

To reduce computation cost for each initial, we compute pair-wise affinity (Eq. 1) of all feature candidates prior to the optimization searching. The quantitative comparison shows that our method advanced the baseline in all metrics (Tab. 4).

3.1.3 Adaptive Parameter

To improve stage-I performance on various type of images from [5], we introduce three hyper-parameters P_d, P_s, P_θ as adaptive candidate constraints in URP-based search. The three hyper-parameters control the maximum feature distance, maximum feature size ratio, and maximum feature angle difference. P_d sets the maximum feature distance, which controls the granularity of RP detection. P_s sets the maximum size difference among RP-instances. And P_θ sets the maximum orientation difference among objects. The hyper-parameters are adapted for each input image, by a grid search to find the most suitable parameter set that leads to the maximal Ω^* in Eq. 6. By adaptive parameter, the stage-I performance can be improved. See Sec. 4.2.3 for ablation study.

3.2 RESCU Stage-II: RP Instance Extension

Stage-I sometimes suffers from missing RP instances. Hence, we propose a self-supervised stage-II for additional RP instance discovery as Fig. 2 shows.

In stage-II, we first use an off-the-shelf region proposal approach [75] to obtain a large set of proposed regions from the single image. The region proposal is designed to extend the pseudo positive & negative samples for self-learning purpose. We use a feature extractor backbone [76] to extract deep features of each RP instance from multiple RPs detected by stage-I, together with the proposed regions. In deep feature space, the proposed regions are matched with RP instances based on a clustering method DBSCAN [77], for its robustness against outliers. The proposed regions with feature closer to the cluster centers of RP instances, together with RP instances detected by stage-I, will be considered

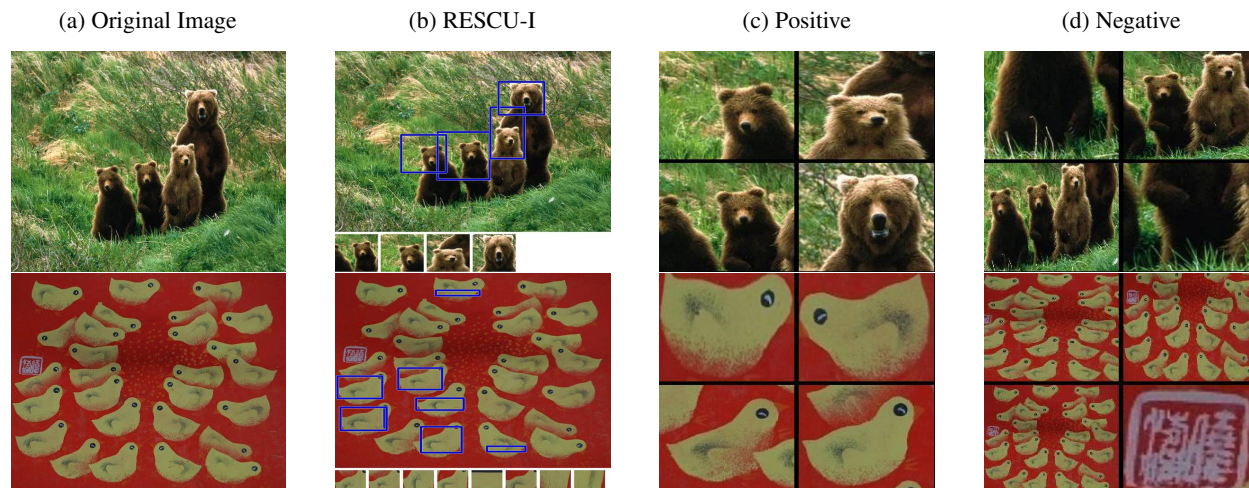


Figure 4: RESCU-II positive & negative samples of some images. (a) Original Image. (b) RESCU-I output. (c) Positive samples generated by RESCU-II. (d) Negative samples generated by RESCU-II.



Figure 5: RESCU-II local Deformation Showcase. Each sample is applied with various deformation factors.

as positive samples. The proposed regions with feature further to those cluster centers will be considered as negative samples.

In practice, we select the top $k = N \times P$ nearest proposals to the cluster centers of RP instances, where N is the number of cluster centers and P is an empirical parameter, set to 40. By this procedure, we maintain $< 10\%$ of the total proposals generated by the off-the-shelf [75]. Fig. 4 shows some example of generated positive & negative samples.

We apply data augmentations to enlarge positive samples for a better training. Besides the general global transformations applied for augmentation, we also apply local appearance & geometric deformation based on corresponding features of RP instances, as Fig. 5 shows. Finally, we apply DenseNet [76], pretrained on Image-Net [78], as the backbone of classifier and append 3 dense layers. We supply implementation details in the Appendix. For each image, it is self-supervised with the obtained positive & negative samples.

4 Experiments & Results

4.1 RP-1K Dataset

The statistics on the Recurring Pattern dataset are in Tab. 3. The RP-1K dataset is collected from several resources: 83 images from [5], 150 images containing perspective deformation from [57], 769 images from [79] and the rest of the images are collected by the authors. Each image is manually labeled using a customized online labeling tool. See sample labeled RPs in Fig. 6.

4.2 Evaluating Unsupervised Recurring Pattern Discovery

4.2.1 Evaluation Metric

We propose two evaluation measurements at Recurring Pattern (RP) and Recurring Pattern Instance (RPI) level respectively :

1) RP instance level: We propose an **intersection-over-detection (IOD)** metric as follows. If RPI_i is a detected RPI, and RPI_{GT_j} a groundtruth RPI. RPI_j is considered acceptable if and only if $(RPI_i \cap RPI_{GT_j})/RPI_i > h$, where h is a numerical threshold. Given a detected RP with a set of RPIs \mathbf{RPI}_D , and some ground truth RP with a set of ground truth RPIs \mathbf{RPI}_{GT} , and the set of acceptable RPIs denoted as \mathbf{RPI}_A , **RP Instance level** precision P_I and recall R_I rates are defined as: $P_I = |\mathbf{RPI}_A|/|\mathbf{RPI}_D|$, $R_I = |\mathbf{RPI}_A|/|\mathbf{RPI}_{GT}|$

Precise segmentation of an object is not the goal of RPD, though human labels (GT RPs) tend to maximize the boundary of each object (Fig. 7) as an RPI. To evaluate RPD output properly, a metric should reward consistently detected overlaps with GT RPs even if the overlaps are partial. The IOD metric captures this correctly while IOU does not (Fig. 7a, 7b, 7c).

We report the evaluation results with threshold $h = 0.5$ in Sec. 4.2.2, 4.2.3. See Appendix Fig. 22 for a detailed study on altering h .

2) RP level: For a detected RP RP_D and all ground truth RPs \mathbf{RP}_{GT} , the one RP_{GT} with the *highest RP instance level precision* P_I is assigned to RP_D . RP_D is considered as an *accepted RP*, denoted as RP_A , if it is assigned to a RP_{GT} . Given multiple RP detections of a single image \mathbf{RP}_D , the ground truth RPs of the same image \mathbf{RP}_{GT} , and the set of *accepted RP* detections \mathbf{RP}_A . **RP level** precision P_{RP} and recall rates R_{RP} are defined as: $P_{RP} = |\mathbf{RP}_A|/|\mathbf{RP}_D|$, $R_{RP} = |\mathbf{RP}_A|/|\mathbf{RP}_{GT}|$.

 Table 3: Statistic of **RP-1K** (with all subsets) and **Grozi-3.2K**

Camera View / RP Category	# Images	# RPs	# Instances	#RP per Image		#Instance per RP	
				Max / Min	Mean \pm STD	Max / Min	Mean \pm STD
Front view	789	4279	16353	24 / 1	5.42 \pm 4.04	96 / 1	3.82 \pm 3.78
Projective view	215	476	2675	17 / 1	2.21 \pm 2.50	75 / 2	5.62 \pm 6.24
Unknown	20	22	174	2 / 1	1.10 \pm 0.30	28 / 2	7.91 \pm 5.59
Man-made rigid	813	3920	16029	24 / 1	4.82 \pm 4.09	96 / 1	4.09 \pm 4.37
Man-made deformable	156	797	2741	16 / 1	5.11 \pm 3.43	28 / 1	3.44 \pm 2.24
Painting	22	26	201	3 / 1	1.18 \pm 0.49	28 / 2	7.73 \pm 5.60
Animal/human	27	28	153	2 / 1	1.04 \pm 0.19	31 / 2	5.46 \pm 6.06
Others	6	6	78	1 / 1	1.00 \pm 0.00	25 / 3	13.00 \pm 8.66
Total of RP-1K	1024	4777	19202	24 / 1	4.67 \pm 3.98	96 / 1	4.02 \pm 4.15
Grozi-3.2K [45]	677	2302	8265	10 / 1	3.40 \pm 1.62	26 / 2	3.59 \pm 2.22

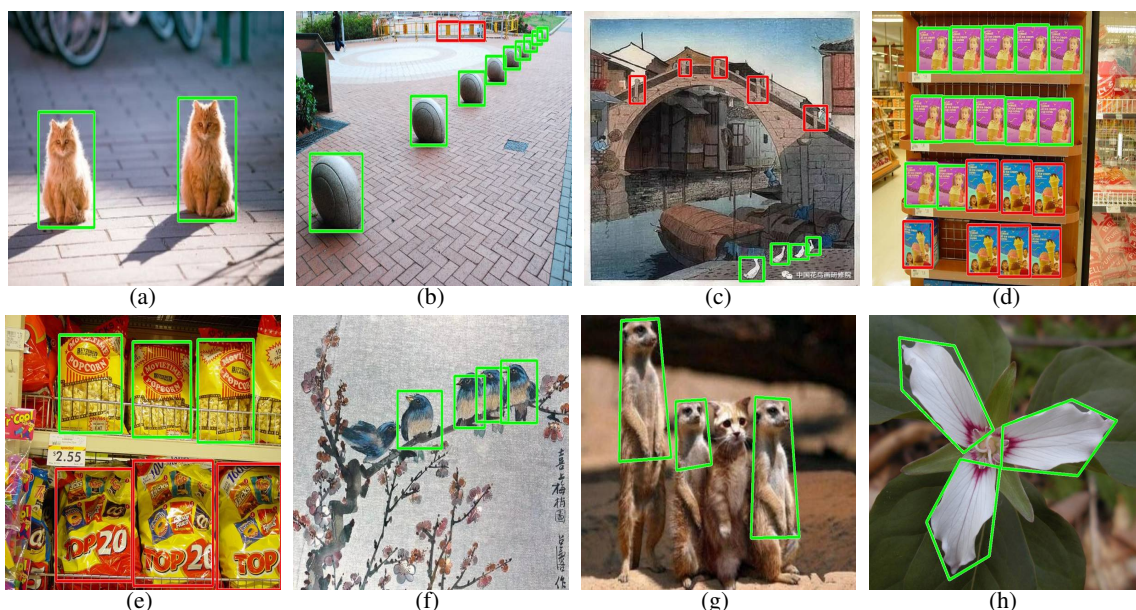


Figure 6: View of the Scene Examples: (a)Frontal, (b)Projective, and (c)Unknown. RP type Examples: (d)Man-made rigid, (e)Man-made deformable, (f)Painting, (g)Animal/human, and (h)Others. The colored contours are human labeled Ground Truth. Zoom in for a more detailed viewing.

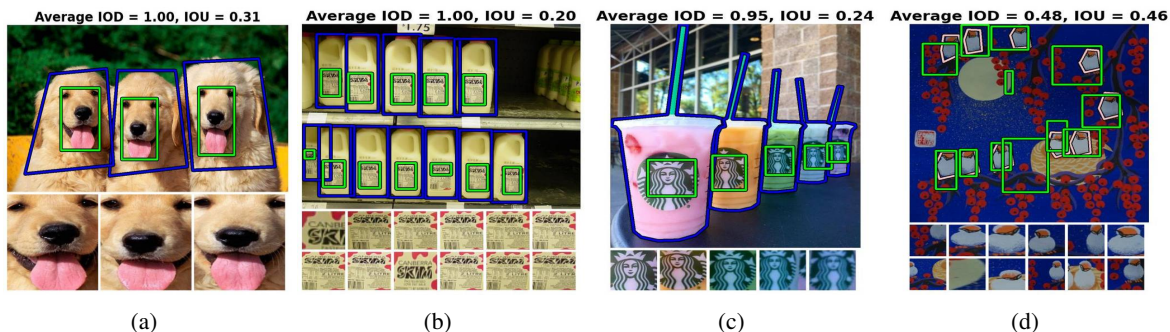


Figure 7: (a,b,c): RPD results on real image examples where both IOD and IOU scores are shown. It is clear that IOD captures the success of RP detection on each image correctly. The partial overlaps detected by RPD are usually the most interesting/complex sub-parts of the objects that recur. (d) demonstrates that large bounding boxes do not hype up IOD scores either. Green: detected RPs. Blue (except (d) pink): GT RPs.

4.2.2 Quantitative Validation

Tab. 4 shows the evaluation on the full **RP-1K** dataset as well as broken down into its various viewpoint and category subsets. Some RP detection examples from each subset category are shown in Fig. 9. All examples shown have **RESCU-II** performs better or as good as **RESCU-I**, and better than the baseline method [5].

Quantitative results of RP detections from Table 4 show that our RESCU outperforms the baseline in both RP and RP Instance level, and especially on the Recall rate. RESCU with stage-II leads to a 2% increase in RP Instance Recall from the baseline. Moreover, our method is able to detect recurring patterns that are missed by human raters. Fig. 8 shows such examples. This observation indicates a limitation on manually labeled **RP-1K** dataset, while also a promise to enhance human RP labels via computational tools such as RESCU.

However, the results from Table 4 also reveal that our RESCU does not perform as well on the Projective view and Man-made deformable subsets. Images from these subsets are usually more challenging for detecting RPs due to severe geometric distortion, non-uniform lighting, and blurring. See Sec. 6.

4.2.3 Ablation Study

As mentioned in Sec. 3.1, here we study the impact of each adaptive parameter.

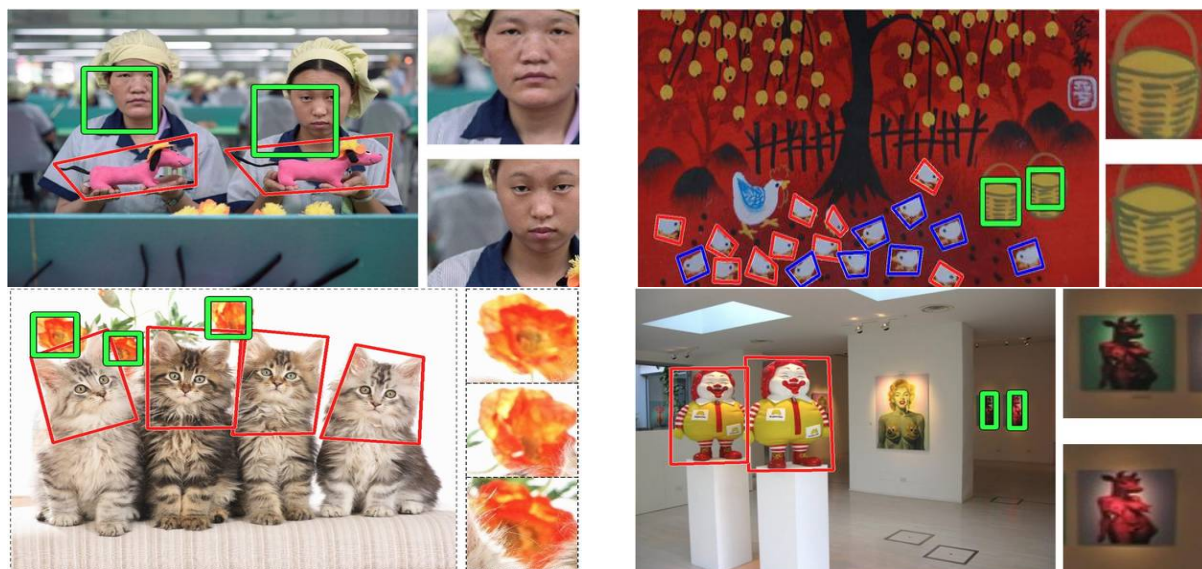


Figure 8: Four sample outputs of our method demonstrate the algorithm’s ability to discover RPs beyond human labels. Green thicker boxes are the detected RP instances by our method, which are not labeled by human raters. The red & blue boxes are human labeled Ground Truth RPs.

Table 4: RP Discovery Evaluation on **RP-1K**. The values in *italic* are not statistically significant with range in the same column section. The values in **bold** are the best mean/std with range in the same column section.

Method	RP Level		RP Instance Level	
	Precision	Recall	Precision	Recall
The Whole RP-1K				
Baseline [5]	0.40 ± 0.37	0.32 ± 0.35	0.67 ± 0.41	0.47 ± 0.38
RESCU-I	0.44 ± 0.32	<i>0.50 ± 0.38</i>	0.68 ± 0.33	0.62 ± 0.34
RESCU-II	0.45 ± 0.32	0.52 ± 0.38	0.71 ± 0.32	0.64 ± 0.33
Front View Subset				
Baseline [5]	0.45 ± 0.36	0.34 ± 0.34	0.73 ± 0.37	0.51 ± 0.36
RESCU-I	0.47 ± 0.30	0.51 ± 0.35	0.70 ± 0.31	0.65 ± 0.32
RESCU-II	0.48 ± 0.31	0.52 ± 0.35	0.73 ± 0.30	0.65 ± 0.32
Projective View Subset				
Baseline [5]	0.23 ± 0.36	0.22 ± 0.37	0.36 ± 0.45	0.27 ± 0.38
RESCU-I	0.32 ± 0.34	0.47 ± 0.45	0.58 ± 0.40	0.44 ± 0.37
RESCU-II	0.33 ± 0.35	0.47 ± 0.45	0.63 ± 0.38	0.49 ± 0.37
Man-Made Rigid Subset				
Baseline [5]	0.42 ± 0.37	0.32 ± 0.35	0.69 ± 0.40	0.49 ± 0.37
RESCU-I	0.44 ± 0.32	0.50 ± 0.37	0.69 ± 0.33	0.62 ± 0.34
RESCU-II	0.45 ± 0.32	0.51 ± 0.37	0.72 ± 0.32	0.63 ± 0.34
Man-Made Deformable Subset				
Baseline [5]	0.33 ± 0.35	0.21 ± 0.26	0.58 ± 0.43	0.43 ± 0.37
RESCU-I	0.38 ± 0.28	0.41 ± 0.33	0.63 ± 0.31	0.63 ± 0.30
RESCU-II	0.40 ± 0.29	0.44 ± 0.33	0.66 ± 0.31	0.63 ± 0.30
Painting Subset				
Baseline [5]	0.45 ± 0.40	0.61 ± 0.48	0.64 ± 0.46	0.34 ± 0.34
RESCU-I	0.73 ± 0.30	0.89 ± 0.29	0.82 ± 0.24	0.60 ± 0.31
RESCU-II	0.74 ± 0.30	0.89 ± 0.29	0.82 ± 0.25	0.60 ± 0.31
Animal/Human Subset				
Baseline [5]	0.45 ± 0.47	0.52 ± 0.50	0.39 ± 0.48	0.25 ± 0.35
RESCU-I	0.57 ± 0.37	0.78 ± 0.42	0.76 ± 0.36	0.59 ± 0.35
RESCU-II	0.62 ± 0.37	0.81 ± 0.39	0.83 ± 0.30	0.67 ± 0.32

Table 5: A Summary of Adaptive Parameters used in RESCU Stage-I.

Adaptive Parameter	Description	Fixed Value	Optimized Values
P_d	the maximum feature distance	0.2	[0.1, 0.15, 0.2]
P_s	the maximum size difference among RP instances	0.5	[0.1, 0.2, 0.3, 0.4, 0.5]
P_θ	the maximum orientation difference among RP instances	30	[30, 90, 180]

- P_d sets the maximum feature distance, which controls the granularity of RP detection.
- P_s sets the maximum size difference among RP instances.
- P_θ sets the maximum orientation difference among RP instances.

To study the impact of these adaptive parameters, we design experiments to separately optimize each parameter (and each pair of two parameters), with fixed other parameters. Tab. 5 shows the fixed value and optimization values of each parameter.

Tab. 6 shows the ablation study of adaptive parameters. From the study we can see that P_d parameter influences the performance most. Fig. 10 shows an example of how changing P_d can control the size of an RP-instance.

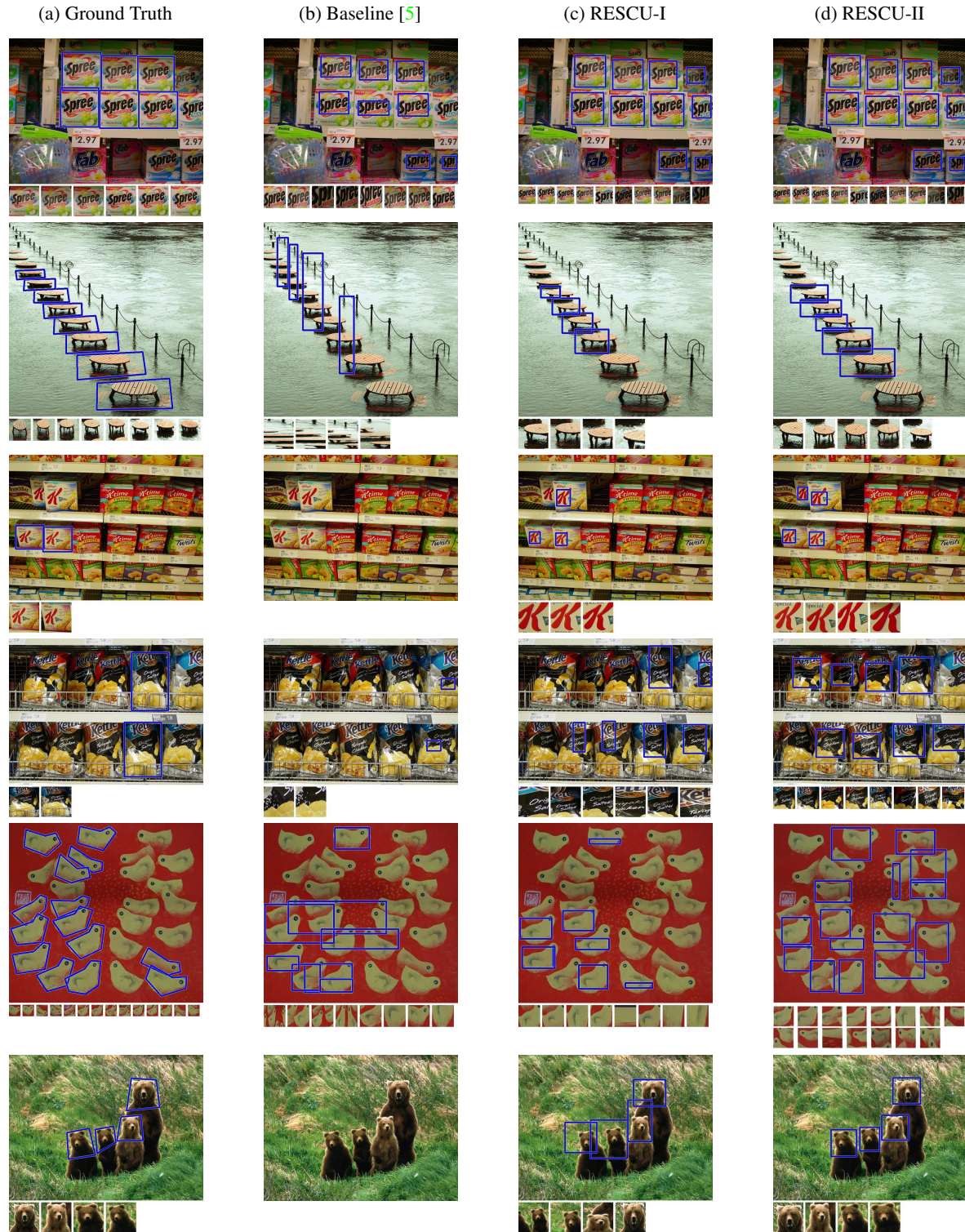


Figure 9: Examples of RP detection results from each camera view/RP category. **Top to Down:** Results broken out by subset categories: Front View, Projective View, Man-Made Rigid, Man-Made Deformable, Painting, Animal/Human subsets.

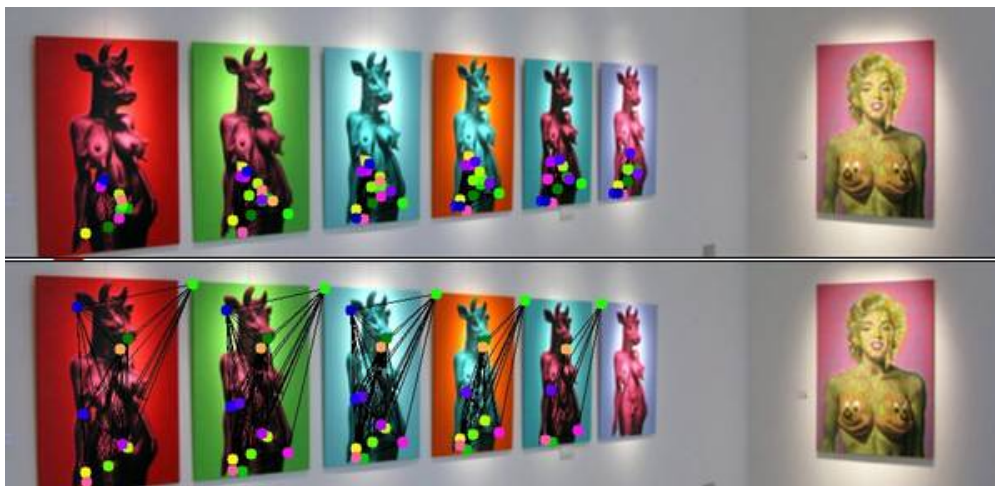


Figure 10: An example of using different P_d in RESCU. **Up**: with $P_d = 0.05$ to detect smaller RP instance, **Down**: with $P_d = 0.25$ to detect larger RP instance.

5 RPD Scene Understanding

5.1 Vanishing Point Detection from A Single View

“Under perspective projection, parallel lines in 3D do not remain parallel but instead meet at the point called *vanishing point* (VP)” [9]. We also emphasize that line segments are not always explicitly visible in real-world images (Fig. 1d). We take advantage of groups of corresponding feature points on detected recurring patterns (Figure 11) to construct and validate the co-linearity of implicit lines and line intersections to find VP through a robust RANSAC procedure.

5.1.1 Line Fitting and RANSAC in Vanishing Point Detection

The intersection of near-parallel lines often results in faulty estimation of the vanishing point. To overcome this ill-conditioning, we introduce an angular constraint (AC) into our algorithm by comparing the angle between lines before selecting them to initialize the RANSAC algorithm. If the angle is smaller (near-parallel lines) than a threshold, we do not consider their contribution towards vanishing point calculation. Using this angular constraint produces a better estimate of the vanishing point. Fig. 12 shows the success rate of our method with and without the Angular Constraint.

5.1.2 Vanishing Point Detection Evaluation

We compare our VP detection method with [57] and a deep learning method for VPD, NeurVPS [58], using public available projective view subset of 147 images with labeled VP ground truth (Fig. 13).

Table 6: Ablation Study of RESCU-I IOD Threshold $h = 0.5$. P_d (maximum RPI feature distance), P_s (maximum RPI size difference), P_θ (maximum RPI orientation difference), See Tab. 5 for parameter details. The values in *italic* are not statistically significant with range in the same column. The values in **bold** are the best mean/std with range in the same column.

Method	P_d	Parameter		RP Level		RP Instance Level	
		P_s	P_θ	Precision	Recall	Precision	Recall
Baseline [5]				0.40 ± 0.37	0.32 ± 0.35	0.67 ± 0.41	0.47 ± 0.38
RESCU-I				0.37 ± 0.31	0.44 ± 0.38	0.70 ± 0.30	0.64 ± 0.32
RESCU-I	✓			0.48 ± 0.33	0.53 ± 0.38	0.73 ± 0.29	0.67 ± 0.32
RESCU-I		✓		0.43 ± 0.33	0.46 ± 0.38	0.72 ± 0.30	0.65 ± 0.32
RESCU-I			✓	0.41 ± 0.33	0.44 ± 0.38	0.67 ± 0.30	0.63 ± 0.32
RESCU-I	✓	✓		<i>0.47</i> ± 0.33	0.53 ± 0.38	0.75 ± 0.28	0.67 ± 0.32
RESCU-I	✓		✓	0.48 ± 0.33	0.53 ± 0.38	0.72 ± 0.29	<i>0.66</i> ± 0.32
RESCU-I		✓	✓	0.43 ± 0.33	0.45 ± 0.38	0.69 ± 0.30	0.64 ± 0.32
RESCU-I	✓	✓	✓	<i>0.47</i> ± 0.34	<i>0.52</i> ± 0.38	0.72 ± 0.29	<i>0.66</i> ± 0.32

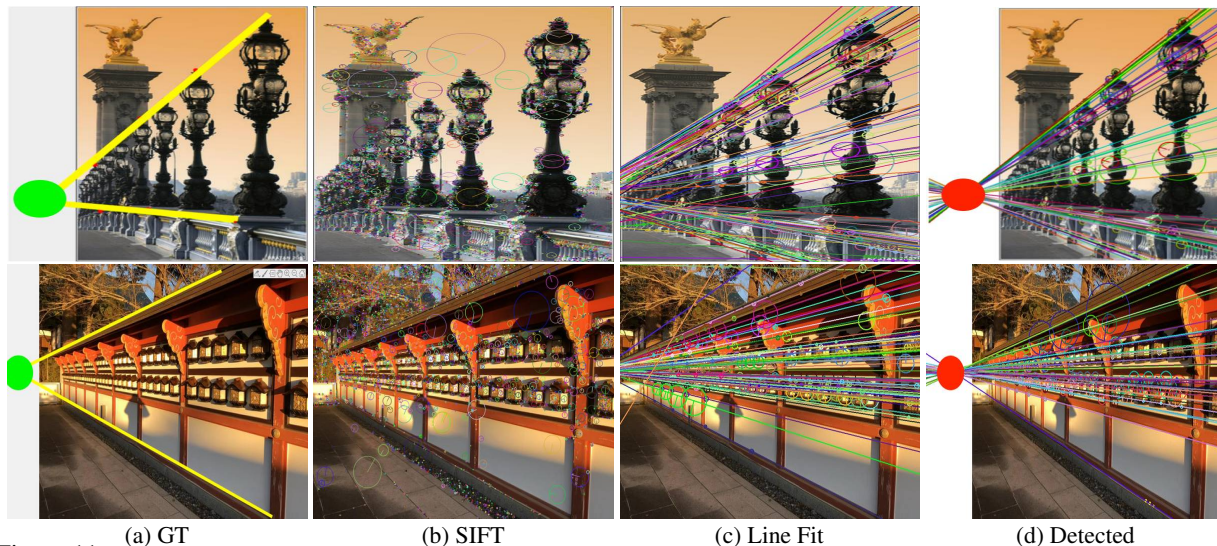


Figure 11: Sample results for VPD. (a) Input image with ground truth, (b) SIFT features extracted, (c) lines fitted to SIFT feature groups, (d) vanishing point detected from our method. More results in supplementary Sec 2.3.

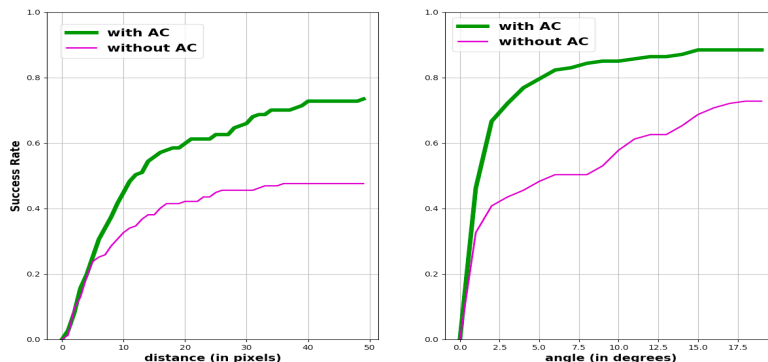


Figure 12: Success rate of vanishing point detection (VPD) with respect to distance (left) and angle (right) difference between predicted and groundtruth VPs. With the introduction of the angular constraint (AC) we see a significant improvement in the performance. The performance of the proposed approach is statistically different with $p\text{-value} = 1.13\text{e-}06$ with the angular constraint.

The success rate (SR) of vanishing point detection is computed as the ratio of number of acceptable vanishing points against ground truth over all the detected vanishing points. We define two methods for comparing a detected VP and the ground truth: a point-based method and a vector-based method. The point-based method compares Euclidean distance in pixels between the 2D VP location (vp_x, vp_y) and the ground truth labeled pixel location, with detections considered accepted if this distance falls within a threshold. In the vector-based method, the VP is represented as a unit vector in the direction $(vp_x - x_0, vp_y - y_0, f)$, where (x_0, y_0) is the image center, and f is a nominal value that would be the camera focal length if known, but otherwise is chosen to be $(\text{image width} + \text{image height})/4$. Distance in this case is the angle between the detected and ground truth VP unit vectors.

Fig. 13 plots the success rate of our method for Euclidean distance (left) and for vector angle (right). We compare our results with NeurVPS [58] and Zhou’s method [57] on a set of 147 images. The baseline method [57] performs poorly on this dataset because it relies on explicit straight line segments in the image to estimate vanishing points. See supplementary Fig.10 12 for more examples with few visually explicit line segments. Our method performs nearly as well as the supervised SOTA method NeurVPS[58], as shown quantitatively in Fig. 13. Our statistical analysis of the results shows that there is no statistically difference on VPD between our method and NeurVPS with $p\text{-values}$ of 0.349 for distance and 0.723 for angle difference.

In addition, we provide the complete results for Vanishing Point (VP) prediction. Fig. 14 shows prediction results from our method separated in columns based on the prediction quality compared with the ground truth. We use angle and distance with respect to the ground truth to assess the prediction quality.

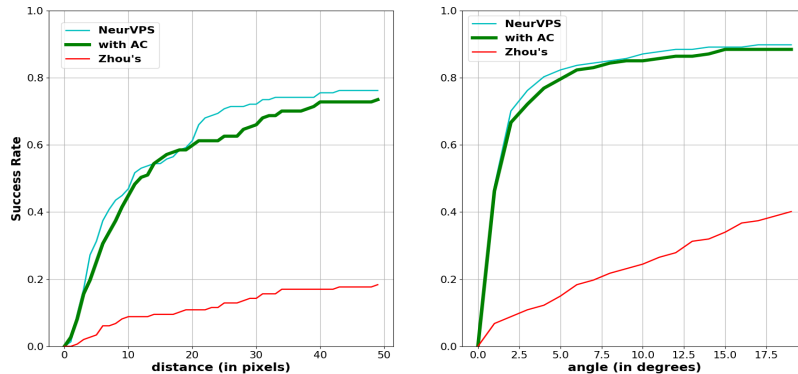


Figure 13: Qualitative analysis of VPD evaluated using distance (left) and angle (right) difference to groundtruth (GTs) respectively. On a test image set of 147 images, we compare our unsupervised recurring pattern based VPD method (Sec. 5.1) with a state-of-the-art deep learning vanishing point detector **NeurVPS** [58], a supervised learning method trained on 270,000 training images. Our statistical analysis of the results show that these two methods have no statistically difference (p -values are 0.349 for distance and 0.723 for angle difference).

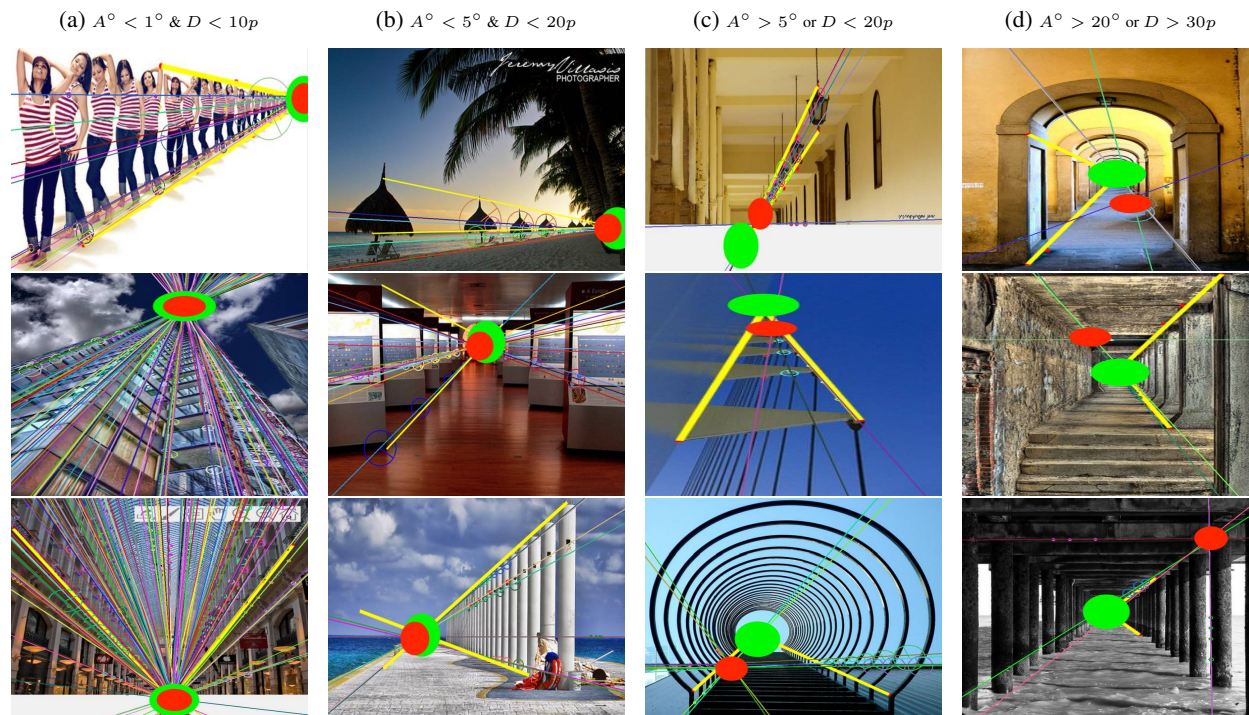


Figure 14: Example vanishing point prediction by our method. A° denotes the vector angle between predicted and ground truth VP vectors in degrees. D represents the distance between predicted and ground truth VP image locations in pixels (p). **Red** dot: our prediction. **Yellow** lines and **Green** dot: two supporting lines intersected at the ground truth vanishing point.

We evaluate our unsupervised recurring pattern based VPD method on a projective view subset of 147 images with labeled VP ground truth and compare it with a state-of-the-art supervised deep learning vanishing point detector **NeurVPS** [58] and another baseline method [57]. Fig. 15 shows the output of the three methods along with the ground truth.

5.2 Translation Symmetry Detection

To further understand and quantify a 3D scene, we investigate the possibility of an RP having 3D translation symmetry. Using projective invariance we are able to detect potential 3D translation symmetry of RP instances in a 2D image. Consider four points A, B, C and D having translation symmetry in 3D space their corresponding projections A', B', C'

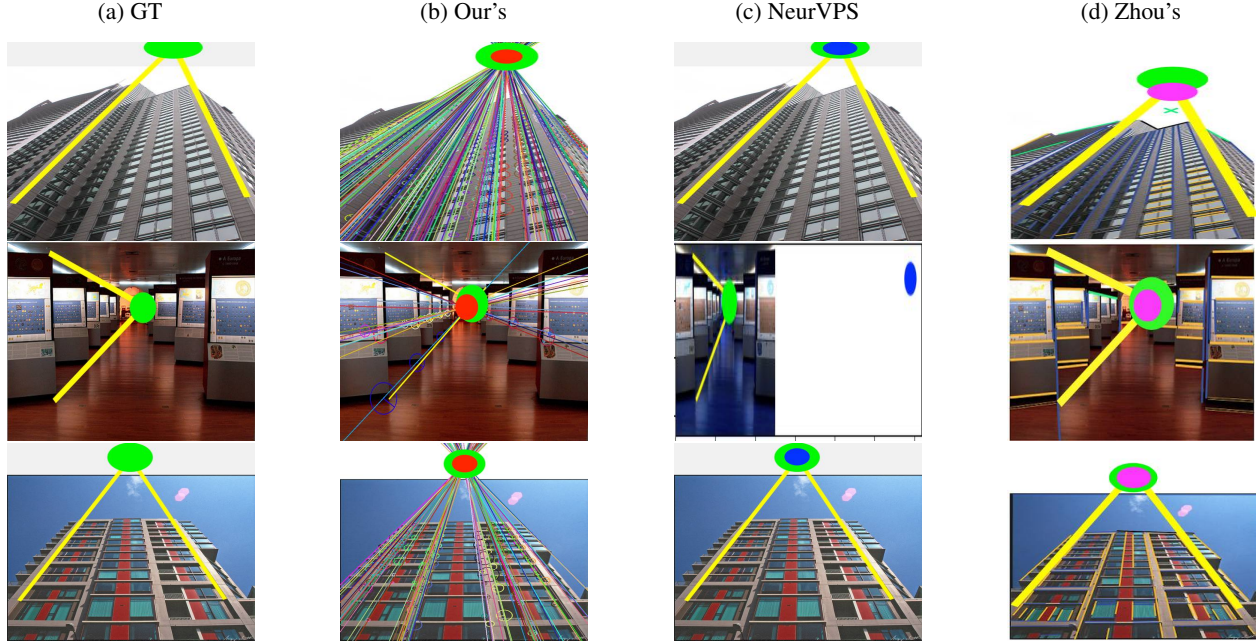


Figure 15: Sample results for vanishing point (VP) detection using our method and a comparison with [58] and [57]. a) Input image with ground truth, b) VP prediction using our method, c) VP prediction using NeurVPS[58], d) VP prediction using Zhou et.al.’s method [57]. **Red** dot: our prediction. **Yellow** lines and **Green** dot: two supporting lines intersected at the ground truth vanishing point. **Blue** is the output of NeurVPS[58] and **Magenta** is the output of Zhou et.al.’s method[57].

and D' on the 2D image as shown in Fig. 16c. By virtue of translation symmetry, $AB = BC = CD = d$ for some 3D translation vector length $\|t\| = d$. The cross ratio, defined as [9]:

$$cr(A, B, C, D) = \frac{AC * BD}{BC * AD} = cr(A', B', C', D') \quad (11)$$

is an invariant value shared by four co-linear 3D points and their 2D image projections regardless of camera position and orientation. For the case of 3D translation symmetry, this computed invariant value will be

$$\frac{AC * BD}{BC * AD} = \frac{(d + d)(d + d)}{d(d + d + d)} = \frac{4}{3}.$$

Fig. 16 evaluates the success rate of translation symmetry for varying thresholds on two different dataset. First, a small translation symmetry ground truth (TS_GT) dataset was created consisting of 12 images (6 synthetic, 6 real images) shown in Fig. 17, for which translation symmetry is known to exist. Second, success rate of translation symmetry was calculated on the VPD dataset. We define success rate for translation symmetry (SR_{ts}) as

$$SR_{ts} = \frac{\# \text{ of images with translation symmetry}}{\# \text{ of images in the dataset}}.$$

The success rate was calculated for varying thresholds in the range $t = (0, 0.15)$ for TS_GT dataset and $t = (0, 1)$ for VPD dataset. It can be seen that success rate reaches a maximum for TS_GT images at the very low threshold of $t = 0.06$

Fig. 17 shows different examples in which translation symmetry was detected from both the aforementioned datasets. Column (a) represents images from TS_GT dataset and column (c) represents images from VPD datasets. Columns to their right represent the rectified outputs of the RPs from their corresponding images. Since URPD is completely unsupervised, we make no assumptions regarding any image. Consequently, we do not have any information regarding the camera parameters with which the image was captured. We maintain this assumption even for the synthetically generated images. Thus the rectified outputs are affine views of the original RPs [10] and therefore, aspect ratios of the rectified outputs do not always match the aspect ratio of the RPs in the real 3D scene (example: first synthetic image of Fig. 17 (row 1, columns 1 and 2)). This is also the case in Fig. 9 of the main paper. It should also be noted that all images in our VPD dataset have translation symmetry of the RPs. But the ground truth for the same is unknown.

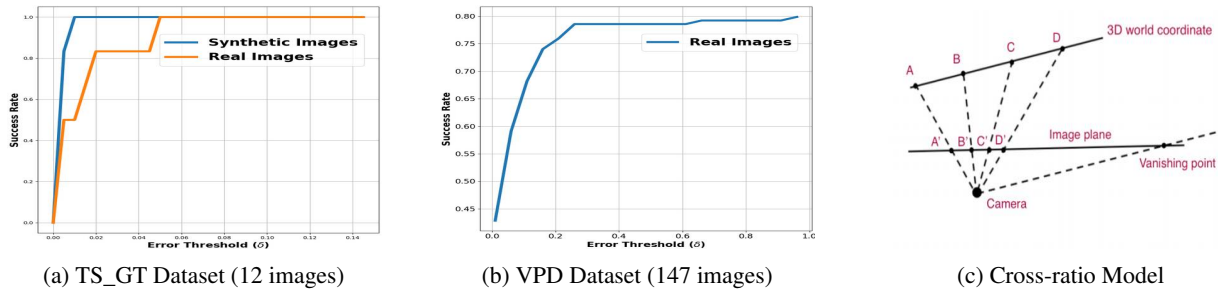


Figure 16: Success rate of our translation symmetry detection for varying thresholds. (a) represents the success rate on a translation symmetry ground truth (TS_GT) dataset consisting of 6 synthetic images and 6 real images for which the translation symmetry is known to exist (example images are shown in Fig. 17). (b) represents the success rate on the VPD dataset with 147 images. (c) represents the cross-ratio model that depicts the relation between the colinear points in the 3D space and their corresponding projections in the 2D image.

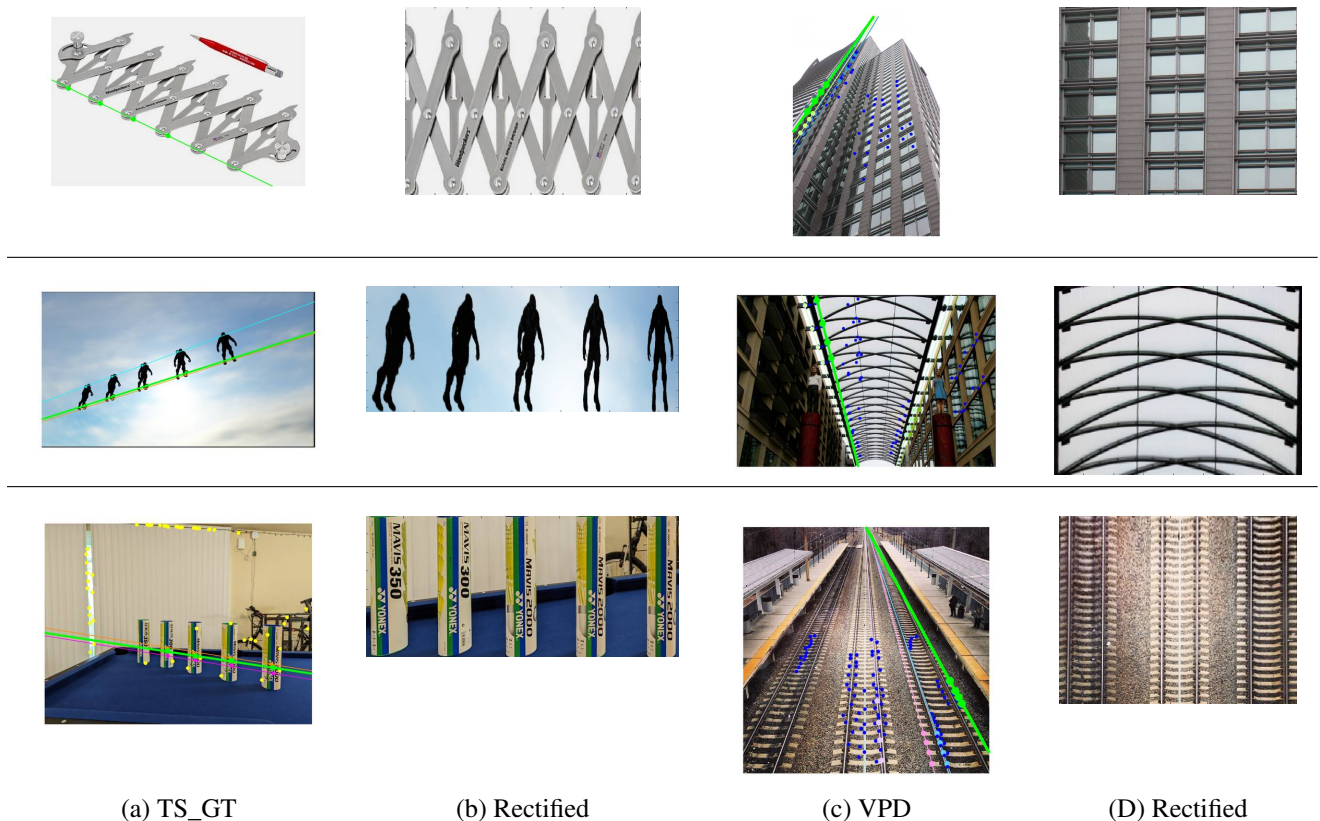


Figure 17: Sample results for translation symmetry detection. (a) represents the original images of the translation symmetry ground truth (TS_GT) dataset for which translation symmetry was known to exist. (b) represents rectified outputs of TS_GT images. (c) represents translation symmetry detected in sample images from VPD dataset, and (d) represents rectified outputs of VPD images.

5.3 RP Instance Counting

RP instance counting differs from object counting that doesn't aim at counting all objects in an image, but focuses on counting the instances that reoccurred. A typical application for RP instance counting is to count number of product belonging to various types, since each type of products can be viewed as an RP for visual similarity, under various lighting conditions, partial occlusion and non-rigid distortion.

Grozi-3.2K[45] with 680 test images is used for evaluation. We apply the fine-grained annotation per product type provided by [80]. We exclude the annotation of certain product types with no RPs. Tab. 3 also shows the RP statistic comparison between **Grozi-3.2K** and our **RP-1K** dataset.

Table 7: RP Discovery Evaluation on **Grozi-3.2K**, IOD Threshold $h = 0.5$. [34] code is not available thus we cannot compare its performance on **RP-1K**. Instance Recall of [34] on **Grozi-3.2K** obtained from Tab. 1 in [34]. The values in *italic* are not statistically significant with each other in the same column.

Method	RP Level		RP Instance Level	
	Precision	Recall	Precision	Recall
Baseline [5]	0.57 ± 0.41	0.37 ± 0.32	0.67 ± 0.38	0.52 ± 0.36
RESCU-I	0.72 ± 0.27	0.73 ± 0.30	0.77 ± 0.27	0.71 ± 0.29
RESCU-II	0.74 ± 0.27	0.73 ± 0.30	0.81 ± 0.26	0.71 ± 0.29
Product Detection [34]	—	—	—	0.72

Tab. 7 shows that our method can achieve a recall rate of over 70% for both RP and RP instance level recall, which indicates the capability of a recurring pattern detection method on counting re-occurred products in a grocery. Comparing with [34] which requires “logo” regions as additional input, RESCU can achieve almost the same RP instance level recall rate.

5.4 Enhanced Image Caption from Detected RPs

Using an off-the-shelf image captioning model, we utilize detected RP information from RESCU to augment generated captions. To achieve this, we employ OFA, a unified multimodal pre-trained network [72]. OFA is a Transformer based, modal-agnostic pre-trained network that has achieved state-of-the-art results in multiple multimodal benchmarks including image captioning. We use the *Large* size OFA model and weights pre-trained on the MS COCO Caption dataset [81] for generating captions.

To enhance the captions obtained from OFA, we assume RP, VP, and TS information has been previously detected for the image. We begin by generating a caption for the image using OFA. We then parse the image’s generated caption for instances of collective nouns such as “group”. If no collective nouns are found, we search the string for noun instances preceded by the word “of”. Finally, we follow a simple grammar to replace collective nouns and words dependent on them with the dominant RP’s count discovered by RESCU. If no collective nouns are detected, we place the RP’s count after “of” and before the detected noun. In addition to enhancing the image caption with RP counts, we add further context by noting potential translation symmetry and whether a detected vanishing point lies inside or outside the image borders. Figure 18 shows example image-caption pairs augmented by our detected RP and VP information. The proposed caption enhancing pipeline is shown in Figure 19.

We further utilize OFA to handle multiple potential RPs and their corresponding nouns in a caption. If the image’s caption contains multiple subject nouns, we use OFA’s visual grounding to ground each detected subject noun in the caption. This gives OFA’s bounding box for the potential region of the text input. We then check the detected RPs overlap with OFA’s proposed region. We assign the corresponding RP to the region and its corresponding noun if the RP’s total area has at least 0.90 overlap with OFA’s proposed region. Figure 20 demonstrates an example image-caption pair enhanced with multiple detected RPs and OFA’s proposed regions for two detected nouns in the image’s caption.

6 Limitations

Fig. 21 shows some limitations of our approach. The method may wrongly detect RP on images with large distortion, non-uniform lighting, and blurring. To address the limitations under these scenarios, our future work approach will be to include additional varying types of extracted initial features to aid and complement the current use of SIFT features. Stage-II will also be improved to enhance the concept of learning similarity under different scenarios.

7 Conclusion

We have illustrated our path from recurrence discovery and representation in a single image as RPs and RP instances to scene understanding in terms of vanishing point, potential 3D translation symmetry and number of recurrences of an unknown “object”. By leveraging some off-the-shelf image caption tools, we demonstrated by examples the feasibility of using knowledge learned from RPs on a single image to produce enhanced, quantitative and detailed captions as . Our 2-stage RESCU differs from all existing unsupervised learning systems in design and which advances the state of the art in URPD. Furthermore, we offer a new benchmark for future URPD algorithm evaluation, and a new RP-based Vanishing Point image set for unsupervised Vanishing Point Discovery (VPD). Our demo video link: [a Demo Video](#)

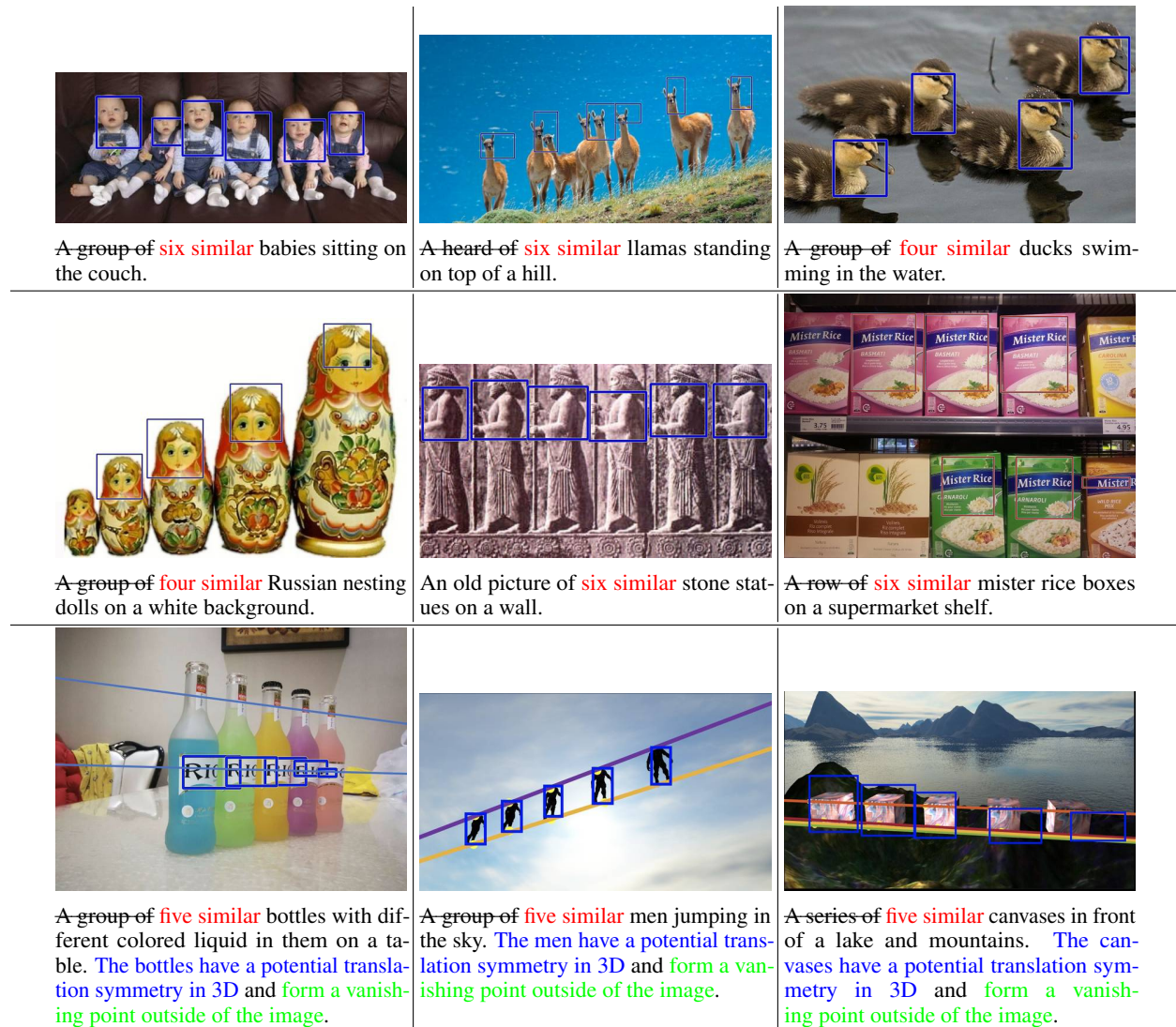


Figure 18: Example image-caption pairs we enhance using detected RP and VP information. The captions below each image contain the original text generated by OFA [72]. We add the dominant RP’s **count** in red following collective nouns. If detected, additional **translation symmetry** and **VP** information is added to the caption.

8 Acknowledgement

This work is supported in part by an NSF grant # 1909315. The authors would like to thank Jesse Scott and Chris Funk for their help during the paper preparation.

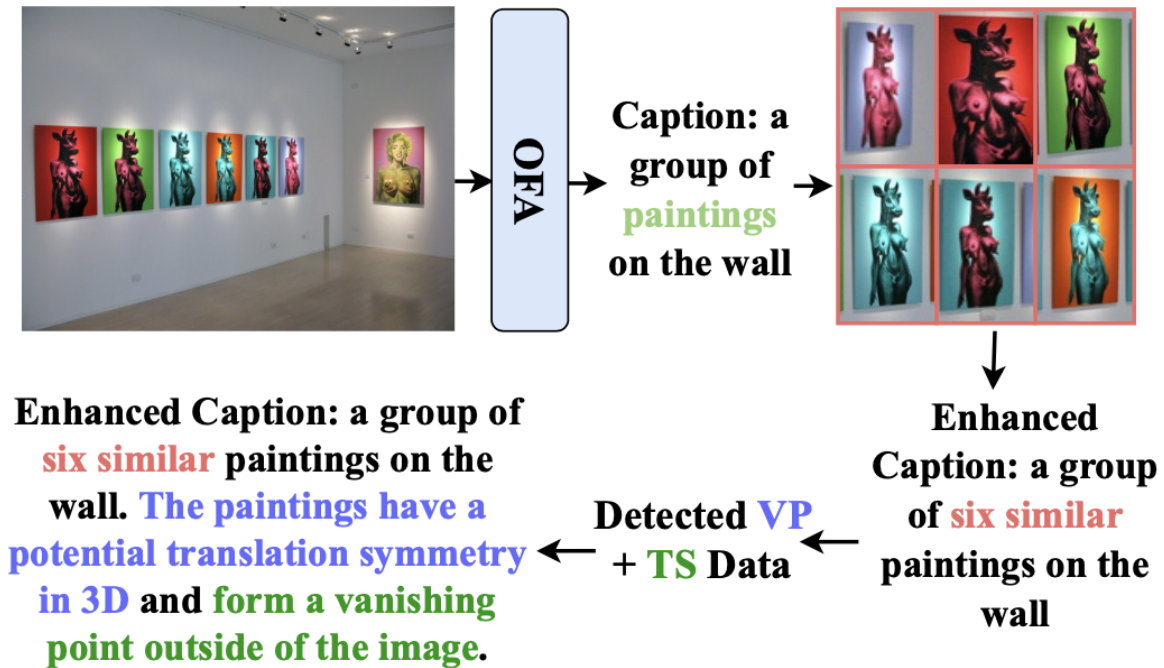


Figure 19: Proposed image caption enhancement pipeline. We obtain image captions using OFA [72]. We parse the sentence for collective nouns or a subject noun and use the previously discovered dominant RP count for that corresponding image to add the detected noun’s count. We further add discovered VP and TS information to the final caption.

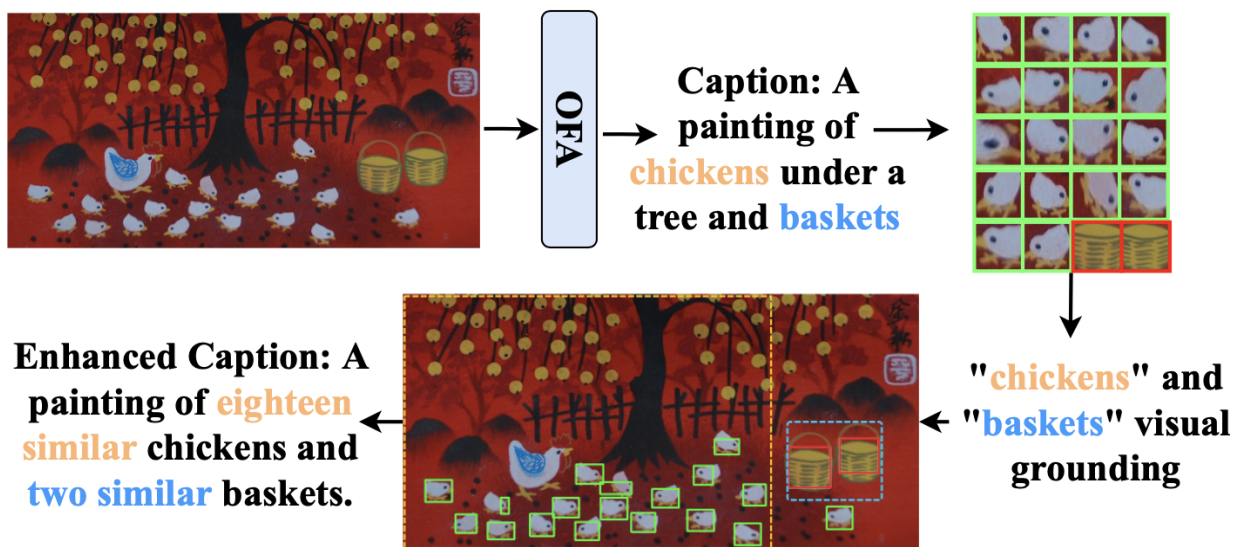


Figure 20: Caption enhancement using two detected RPs. We utilize OFA’s visual grounding for the prompts “chickens” and “baskets” to determine which noun subject the RP is most likely to corresponds with.

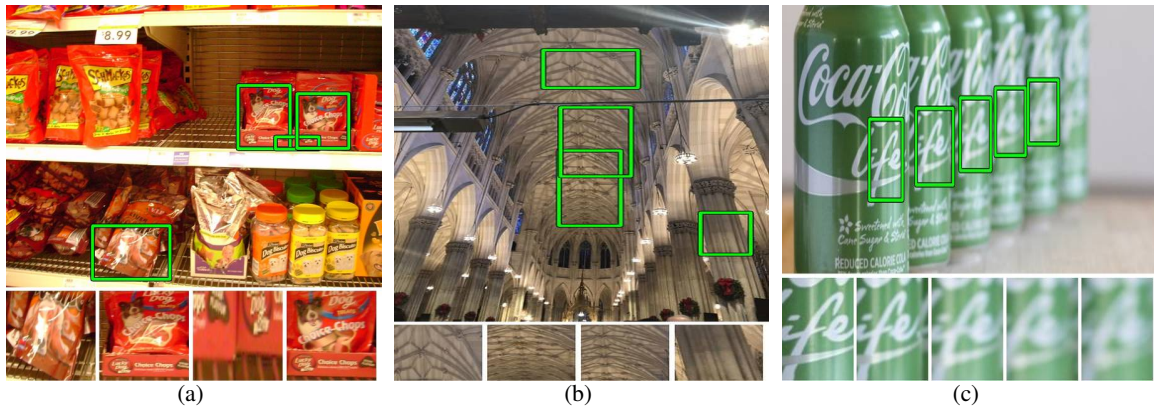


Figure 21: Limitations of RESCU. **(a)** Wrongly involves dissimilar RP instance due to deformation and non-uniform lighting. **(b)** Wrongly involves dissimilar RP instance due to the interference of texture. **(c)** Misses the furthest RP instance due to blurring.

References

- [1] Li, Y., Pizlo, Z., Steinman, R.M.: A computational model that recovers the 3d shape of an object from a single 2d retinal representation. *Vision research* **49** (2009) 979–991 [1](#)
- [2] Treder, M.S.: Behind the looking-glass: A review on human symmetry perception. *Symmetry* **2** (2010) 1510–1543 [1](#)
- [3] Michaux, A., Jayadevan, V., Delp III, E.J., Pizlo, Z.: Figure-ground organization based on three-dimensional symmetry. *Journal of Electronic Imaging* **25** (2016) 1–11 [1](#)
- [4] Sawada, T., Li, Y., Pizlo, Z.: Detecting 3-d mirror symmetry in a 2-d camera image for 3-d shape recovery. *Proceedings of the IEEE* **102** (2014) 1588–1606 [1](#)
- [5] Liu, J., Liu, Y.: Grasp recurring patterns from a single view. In: 2013 IEEE Conference on Computer Vision and Pattern Recognition. (2013) 2003–2010 [1](#), [2](#), [3](#), [4](#), [6](#), [7](#), [9](#), [10](#), [11](#), [12](#), [17](#), [26](#)
- [6] Mitra, N.J., Guibas, L.J., Pauly, M.: Partial and approximate symmetry detection for 3d geometry. *ACM Transactions on Graphics (TOG)* **25** (2006) 560–568 [1](#)
- [7] Liu, H., Yan, S.: Common visual pattern discovery via spatially coherent correspondences. In: 2010 IEEE Computer Society Conference on Computer Vision and Pattern Recognition, IEEE (2010) 1609–1616 [1](#), [2](#)
- [8] Mattson, M.P.: Superior pattern processing is the essence of the evolved human brain. *Frontiers in neuroscience* **8** (2014) 1–17 [1](#)
- [9] Mundy, J.L., Zisserman, A., eds.: *Geometric Invariance in Computer Vision*. MIT Press, Cambridge, MA, USA (1992) [1](#), [3](#), [12](#), [15](#)
- [10] Schaffalitzky, F., Zisserman, A.: Planar grouping for automatic detection of vanishing lines and points. *Image and Vision Computing* **8** (2000) 647–658 [1](#), [3](#), [15](#)
- [11] Weyl, H.: *Symmetry*. Volume 47. Princeton University Press (2015) [1](#)
- [12] Criminisi, A., Reid, I., Zisserman, A.: Single view metrology. *International Journal of Computer Vision* **40** (2000) 123–148 [1](#)
- [13] Zhu, R., Yang, X., Hold-Geoffroy, Y., Perazzi, F., Eisenmann, J., Sunkavalli, K., Chandraker, M.: Single view metrology in the wild. In: Vedaldi, A., Bischof, H., Brox, T., Frahm, J.M., eds.: *Computer Vision – ECCV 2020*, Cham, Springer International Publishing (2020) 316–333 [1](#)
- [14] Cho, M., Lee, J., Lee, K.M.: Reweighted random walks for graph matching. In: *European conference on Computer vision*, Springer (2010) 492–505 [2](#)
- [15] Rother, C., Minka, T., Blake, A., Kolmogorov, V.: Cosegmentation of image pairs by histogram matching—incorporating a global constraint into mrfs. In: 2006 IEEE Computer Society Conference on Computer Vision and Pattern Recognition (CVPR’06). Volume 1., IEEE (2006) 993–1000 [2](#)
- [16] Toshev, A., Shi, J., Daniilidis, K.: Image matching via saliency region correspondences. In: 2007 IEEE Conference on Computer Vision and Pattern Recognition, IEEE (2007) 1–8 [2](#)
- [17] Kannala, J., Rahtu, E., Brandt, S.S., Heikkila, J.: Object recognition and segmentation by non-rigid quasi-dense matching. In: 2008 IEEE Conference on Computer Vision and Pattern Recognition, IEEE (2008) 1–8 [2](#)
- [18] Yuan, J., Wu, Y.: Spatial random partition for common visual pattern discovery. In: 2007 IEEE 11th International Conference on Computer Vision, IEEE (2007) 1–8 [2](#)
- [19] Cho, M., Shin, Y.M., Lee, K.M.: Co-recognition of image pairs by data-driven monte carlo image exploration. In: *European conference on computer vision*, Springer (2008) 144–157 [2](#)
- [20] Cho, M., Lee, J., Lee, K.M.: Feature correspondence and deformable object matching via agglomerative correspondence clustering. In: 2009 IEEE 12th International Conference on Computer Vision, IEEE (2009) 1280–1287 [2](#)
- [21] Cho, M., Shin, Y.M., Lee, K.M.: Unsupervised detection and segmentation of identical objects. In: 2010 IEEE Computer Society Conference on Computer Vision and Pattern Recognition, IEEE (2010) 1617–1624 [2](#)
- [22] Gao, J., Hu, Y., Liu, J., Yang, R.: Unsupervised learning of high-order structural semantics from images. In: 2009 IEEE 12th International Conference on Computer Vision, IEEE (2009) 2122–2129 [2](#)
- [23] Rubinstein, M., Joulain, A., Kopf, J., Liu, C.: Unsupervised joint object discovery and segmentation in internet images. In: *Proceedings of the IEEE conference on computer vision and pattern recognition*. (2013) 1939–1946 [2](#)

- [24] Hong, Y., Si, Z., Hu, W., Zhu, S.C., Wu, Y.N.: Unsupervised learning of compositional sparse code for natural image representation. *Quarterly of Applied Mathematics* (2014) 373–406 [2](#)
- [25] Faktor, A., Irani, M.: “clustering by composition”—unsupervised discovery of image categories. *IEEE transactions on pattern analysis and machine intelligence* **36** (2013) 1092–1106 [2](#)
- [26] Sivic, J., Russell, B.C., Zisserman, A., Freeman, W.T., Efros, A.A.: Unsupervised discovery of visual object class hierarchies. In: 2008 IEEE Conference on Computer Vision and Pattern Recognition, IEEE (2008) 1–8 [2](#)
- [27] Todorovic, S., Ahuja, N.: Unsupervised category modeling, recognition, and segmentation in images. *IEEE Transactions on Pattern Analysis and Machine Intelligence* **30** (2008) 2158–2174 [2](#)
- [28] Fergus, R., Perona, P., Zisserman, A.: Object class recognition by unsupervised scale-invariant learning. In: 2003 IEEE Computer Society Conference on Computer Vision and Pattern Recognition, 2003. Proceedings. Volume 2., IEEE (2003) 1–8 [2](#)
- [29] Vo, V.H., Sizikova, E., Schmid, C., Pérez, P., Ponce, J.: Large-scale unsupervised object discovery. *Advances in Neural Information Processing Systems* **34** (2021) 16764–16778 [2](#)
- [30] Vo, H.V., Pérez, P., Ponce, J.: Toward unsupervised, multi-object discovery in large-scale image collections. In: *European Conference on Computer Vision*, Springer (2020) 779–795 [2](#)
- [31] Huberman, I., Fattal, R.: Detecting repeating objects using patch correlation analysis. In: 2016 IEEE Conference on Computer Vision and Pattern Recognition (CVPR), Los Alamitos, CA, USA, IEEE Computer Society (2016) 2903–2911 [2](#)
- [32] Lettry, L., Perdoch, M., Vanhoey, K., Van Gool, L.: Repeated pattern detection using cnn activations. In: 2017 IEEE Winter Conference on Applications of Computer Vision (WACV), IEEE (2017) 47–55 [2](#)
- [33] Rodríguez-Pardo, C., Suja, S., Pascual, D., Lopez-Moreno, J., Garces, E.: Automatic extraction and synthesis of regular repeatable patterns. *Computers & Graphics* **83** (2019) 33–41 [2](#)
- [34] Geng, W., Han, F., Lin, J., Zhu, L., Bai, J., Wang, S., He, L., Xiao, Q., Lai, Z.: Fine-grained grocery product recognition by one-shot learning. In: *Proceedings of the 26th ACM international conference on Multimedia*. (2018) 1706–1714 [2](#), [3](#), [4](#), [17](#)
- [35] Zhang, Z., Jing, T., Tian, C., Cui, P., Li, X., Gao, M.: Objects discovery based on co-occurrence word model with anchor-box polishing. *IEEE Transactions on Circuits and Systems for Video Technology* **30** (2019) 632–645 [2](#)
- [36] Shi, M., Lu, H., Feng, C., Liu, C., Cao, Z.: Represent, compare, and learn: A similarity-aware framework for class-agnostic counting. In: *Proceedings of the IEEE/CVF Conference on Computer Vision and Pattern Recognition*. (2022) 9529–9538 [2](#), [4](#)
- [37] Cho, M., Kwak, S., Schmid, C., Ponce, J.: Unsupervised object discovery and localization in the wild: Part-based matching with bottom-up region proposals. In: *Proceedings of the IEEE conference on computer vision and pattern recognition*. (2015) 1201–1210 [2](#)
- [38] Wei, X.S., Zhang, C.L., Wu, J., Shen, C., Zhou, Z.H.: Unsupervised object discovery and co-localization by deep descriptor transformation. *Pattern Recognition* **88** (2019) 113–126 [2](#)
- [39] Siméoni, O., Puy, G., Vo, H.V., Roburin, S., Gidaris, S., Bursuc, A., Pérez, P., Marlet, R., Ponce, J.: Localizing objects with self-supervised transformers and no labels. In: *BMVC*. (2021) [2](#)
- [40] Noroozi, M., Favaro, P.: Unsupervised learning of visual representations by solving jigsaw puzzles. In: *European conference on computer vision*, Springer (2016) 69–84 [3](#)
- [41] Misra, I., Maaten, L.v.d.: Self-supervised learning of pretext-invariant representations. In: *Proceedings of the IEEE/CVF Conference on Computer Vision and Pattern Recognition*. (2020) 6707–6717 [3](#)
- [42] Pathak, D., Krahenbuhl, P., Donahue, J., Darrell, T., Efros, A.A.: Context encoders: Feature learning by inpainting. In: *Proceedings of the IEEE conference on computer vision and pattern recognition*. (2016) 2536–2544 [3](#)
- [43] Lin, T.Y., Maire, M., Belongie, S., Hays, J., Perona, P., Ramanan, D., Dollár, P., Zitnick, C.L.: Microsoft coco: Common objects in context. *Computer Vision – ECCV 2014* **8693** (2014) 740—755 [3](#)
- [44] Everingham, M., Van Gool, L., Williams, C.K., Winn, J., Zisserman, A.: The pascal visual object classes (voc) challenge. *International journal of computer vision* **88** (2010) 303–338 [3](#)
- [45] George, M., Floerkemeier, C.: Recognizing products: A per-exemplar multi-label image classification approach. In: *European Conference on Computer Vision*, Springer (2014) 440–455 [3](#), [8](#), [16](#)
- [46] Hsieh, M.R., Lin, Y.L., Hsu, W.H.: Drone-based object counting by spatially regularized regional proposal network. In: *Proceedings of the IEEE international conference on computer vision*. (2017) 4145–4153 [3](#)

- [47] Cordts, M., Omran, M., Ramos, S., Rehfeld, T., Enzweiler, M., Benenson, R., Franke, U., Roth, S., Schiele, B.: The cityscapes dataset for semantic urban scene understanding. In: Proceedings of the IEEE conference on computer vision and pattern recognition. (2016) 3213–3223 [3](#)
- [48] Patil, V., Sakaridis, C., Liniger, A., Van Gool, L.: P3depth: Monocular depth estimation with a piecewise planarity prior. In: Proceedings of the IEEE/CVF Conference on Computer Vision and Pattern Recognition. (2022) 1610–1621 [3](#)
- [49] Li, Z., Wang, X., Liu, X., Jiang, J.: Binsformer: Revisiting adaptive bins for monocular depth estimation. arXiv preprint arXiv:2204.00987 (2022) [3](#)
- [50] Yan, J., Zhao, H., Bu, P., Jin, Y.: Channel-wise attention-based network for self-supervised monocular depth estimation. In: 2021 International Conference on 3D Vision (3DV), IEEE (2021) 464–473 [3](#)
- [51] Wang, H., Zhang, C., Yu, J., Cai, W.: Spatiality-guided transformer for 3d dense captioning on point clouds. arXiv preprint arXiv:2204.10688 (2022) [3](#)
- [52] Azuma, D., Miyanishi, T., Kurita, S., Kawanabe, M.: Scanqa: 3d question answering for spatial scene understanding. In: Proceedings of the IEEE/CVF Conference on Computer Vision and Pattern Recognition. (2022) 19129–19139 [3](#)
- [53] Xu, J., De Mello, S., Liu, S., Byeon, W., Breuel, T., Kautz, J., Wang, X.: Groupvit: Semantic segmentation emerges from text supervision. In: Proceedings of the IEEE/CVF Conference on Computer Vision and Pattern Recognition. (2022) 18134–18144 [3](#)
- [54] Lambert, J., Liu, Z., Sener, O., Hays, J., Koltun, V.: Mseg: A composite dataset for multi-domain semantic segmentation. In: Proceedings of the IEEE/CVF conference on computer vision and pattern recognition. (2020) 2879–2888 [3](#)
- [55] Rother, C.: A new approach to vanishing point detection in architectural environments. *Image and Vision Computing* **20** (2002) 647–655 [3](#)
- [56] Shi, J., Wang, J., Fu, F.: Fast and robust vanishing point detection for unstructured road following. *IEEE Transactions on Intelligent Transportation Systems* **17** (2015) 970–979 [3](#)
- [57] Zhou, Z., Farhat, F., Wang, J.Z.: Detecting dominant vanishing points in natural scenes with application to composition-sensitive image retrieval. *IEEE Transactions on Multimedia* **19** (2017) 2651–2665 [3](#), [7](#), [12](#), [13](#), [14](#), [15](#)
- [58] Zhou, Y., Qi, H., Huang, J., Ma, Y. In: *NeurVPS: Neural Vanishing Point Scanning via Conic Convolution*. Volume 32. Curran Associates Inc., Red Hook, NY, USA (2019) [3](#), [12](#), [13](#), [14](#), [15](#)
- [59] Mundy, J.L., Zisserman, A.: Repeated structures: Image correspondence constraints and 3d structure recovery. In: *Joint European-US Workshop on Applications of Invariance in Computer Vision*, Springer (1993) 89–106 [3](#)
- [60] Goldman, E., Herzig, R., Eisenschat, A., Goldberger, J., Hassner, T.: Precise detection in densely packed scenes. In: Proceedings of the IEEE/CVF Conference on Computer Vision and Pattern Recognition. (2019) 5227–5236 [4](#)
- [61] Lin, T.Y., Goyal, P., Girshick, R., He, K., Dollár, P.: Focal loss for dense object detection. In: Proceedings of the IEEE international conference on computer vision. (2017) 2980–2988 [4](#)
- [62] Lei, Y., Liu, Y., Zhang, P., Liu, L.: Towards using count-level weak supervision for crowd counting. *Pattern Recognition* **109** (2021) 107616 [4](#)
- [63] Lu, E., Xie, W., Zisserman, A.: Class-agnostic counting. In: *Asian conference on computer vision*, Springer (2018) 669–684 [4](#)
- [64] Ranjan, V., Sharma, U., Nguyen, T., Hoai, M.: Learning to count everything. In: Proceedings of the IEEE/CVF Conference on Computer Vision and Pattern Recognition. (2021) 3394–3403 [4](#)
- [65] Hobley, M., Prisacariu, V.: Learning to count anything: Reference-less class-agnostic counting with weak supervision. arXiv preprint arXiv:2205.10203 (2022) [4](#)
- [66] Zhang, Y., Shao, L., Snoek, C.G.: Repetitive activity counting by sight and sound. In: Proceedings of the IEEE/CVF Conference on Computer Vision and Pattern Recognition. (2021) 14070–14079 [4](#)
- [67] Dwibedi, D., Aytar, Y., Tompson, J., Sermanet, P., Zisserman, A.: Counting out time: Class agnostic video repetition counting in the wild. In: Proceedings of the IEEE/CVF conference on computer vision and pattern recognition. (2020) 10387–10396 [4](#)
- [68] Stefanini, M., Cornia, M., Baraldi, L., Cascianelli, S., Fiameni, G., Cucchiara, R.: From show to tell: A survey on deep learning-based image captioning. *IEEE Transactions on Pattern Analysis and Machine Intelligence* (2022) 1–20 [4](#)

- [69] Ren, S., He, K., Girshick, R., Sun, J.: Faster r-cnn: Towards real-time object detection with region proposal networks. In Cortes, C., Lawrence, N., Lee, D., Sugiyama, M., Garnett, R., eds.: *Advances in Neural Information Processing Systems*. Volume 28., Curran Associates, Inc. (2015) 4
- [70] Anderson, P., He, X., Buehler, C., Teney, D., Johnson, M., Gould, S., Zhang, L.: Bottom-up and top-down attention for image captioning and visual question answering. In: *Proceedings of the IEEE conference on computer vision and pattern recognition*. (2018) 6077–6086 4
- [71] Li, X., Yin, X., Li, C., Zhang, P., Hu, X., Zhang, L., Wang, L., Hu, H., Dong, L., Wei, F., et al.: Oscar: Object-semantics aligned pre-training for vision-language tasks. In: *European Conference on Computer Vision*, Springer (2020) 121–137 4
- [72] Wang, P., Yang, A., Men, R., Lin, J., Bai, S., Li, Z., Ma, J., Zhou, C., Zhou, J., Yang, H.: Unifying modalities, tasks, and architectures through a simple sequence-to-sequence learning framework. In: *Proceedings of the 39th International Conference on Machine Learning, ICML 2022*. *Proceedings of Machine Learning Research*, PMLR (2022) 4, 17, 18, 19
- [73] Zhou, L., Palangi, H., Zhang, L., Hu, H., Corso, J., Gao, J.: Unified vision-language pre-training for image captioning and vqa. *Proceedings of the AAAI Conference on Artificial Intelligence* 34 (2020) 13041–13049 4
- [74] Feo, T.A., Resende, M.G.: Greedy randomized adaptive search procedures. *Journal of global optimization* 6 (1995) 109–133 6
- [75] Zitnick, C.L., Dollár, P.: Edge boxes: Locating object proposals from edges. In Fleet, D., Pajdla, T., Schiele, B., Tuytelaars, T., eds.: *European Conference on Computer Vision*, Cham, Springer International Publishing (2014) 391–405 6, 7
- [76] Huang, G., Liu, Z., Van Der Maaten, L., Weinberger, K.Q.: Densely connected convolutional networks. In: *Proceedings of the IEEE conference on computer vision and pattern recognition*. (2017) 4700–4708 6, 7
- [77] Ester, M., Kriegel, H.P., Sander, J., Xu, X.: A density-based algorithm for discovering clusters in large spatial databases with noise. In: *Proceedings of the Second International Conference on Knowledge Discovery and Data Mining*. KDD'96, AAAI Press (1996) 226—231 6
- [78] Deng, J., Dong, W., Socher, R., Li, L.J., Li, K., Fei-Fei, L.: Imagenet: A large-scale hierarchical image database. In: *2009 IEEE conference on computer vision and pattern recognition, Ieee* (2009) 248–255 7
- [79] Zhang, Y., Wang, L., Hartley, R., Li, H.: Handling significant scale difference for object retrieval in a supermarket. In: *2009 Digital Image Computing: Techniques and Applications, IEEE* (2009) 468–475 7
- [80] Osokin, A., Sumin, D., Lomakin, V.: Os2d: One-stage one-shot object detection by matching anchor features. In: *European Conference on Computer Vision*, Springer (2020) 635–652 16
- [81] Chen, X., Fang, H., Lin, T.Y., Vedantam, R., Gupta, S., Dollár, P., Zitnick, C.L.: Microsoft coco captions: Data collection and evaluation server. *arXiv preprint arXiv:1504.00325* (2015) 17
- [82] Kingma, D.P., Ba, J.: Adam: A method for stochastic optimization. *arXiv preprint arXiv:1412.6980* (2014) 25

9 Appendix

9.1 Varying IOD Threshold

To study the effect of different values of IOD threshold h , Figure 22 shows the performance metrics plotted with respect to increasing values of IOD threshold h . We observe that the trends of both RP level and RP-Instance level metrics monotonically decrease with increasing h . Moreover, the RP recall rate and Instance precision & recall rates are mostly flat when h changes. This indicates that most metrics are not losing correctness when altering h value. These results further support the conclusion that our **RESCU** method performs quantitatively better than the **baseline**.

9.2 Implementation Details

During training we utilize the Adam [82] optimizer with Cross-Entropy loss. We use $1e^{-4}$ as our learning rate with a 0.5 decay rate. We train for a maximum of 20 epochs using a batch size of 32 and apply early stopping if validation loss does not decrease by $5e^{-4}$ over three iterations.

9.3 Demo Video

Fig. 23 shows the demo video representative frames of four showcases, including results of RESCU-I, RESCU-II, vanishing point detection, translation symmetry detection, enhanced image caption, image rectification, and 3D scene visualization based on RP discovery.

Novel 3D Scene Understanding Applications From Recurrence in a Single Image

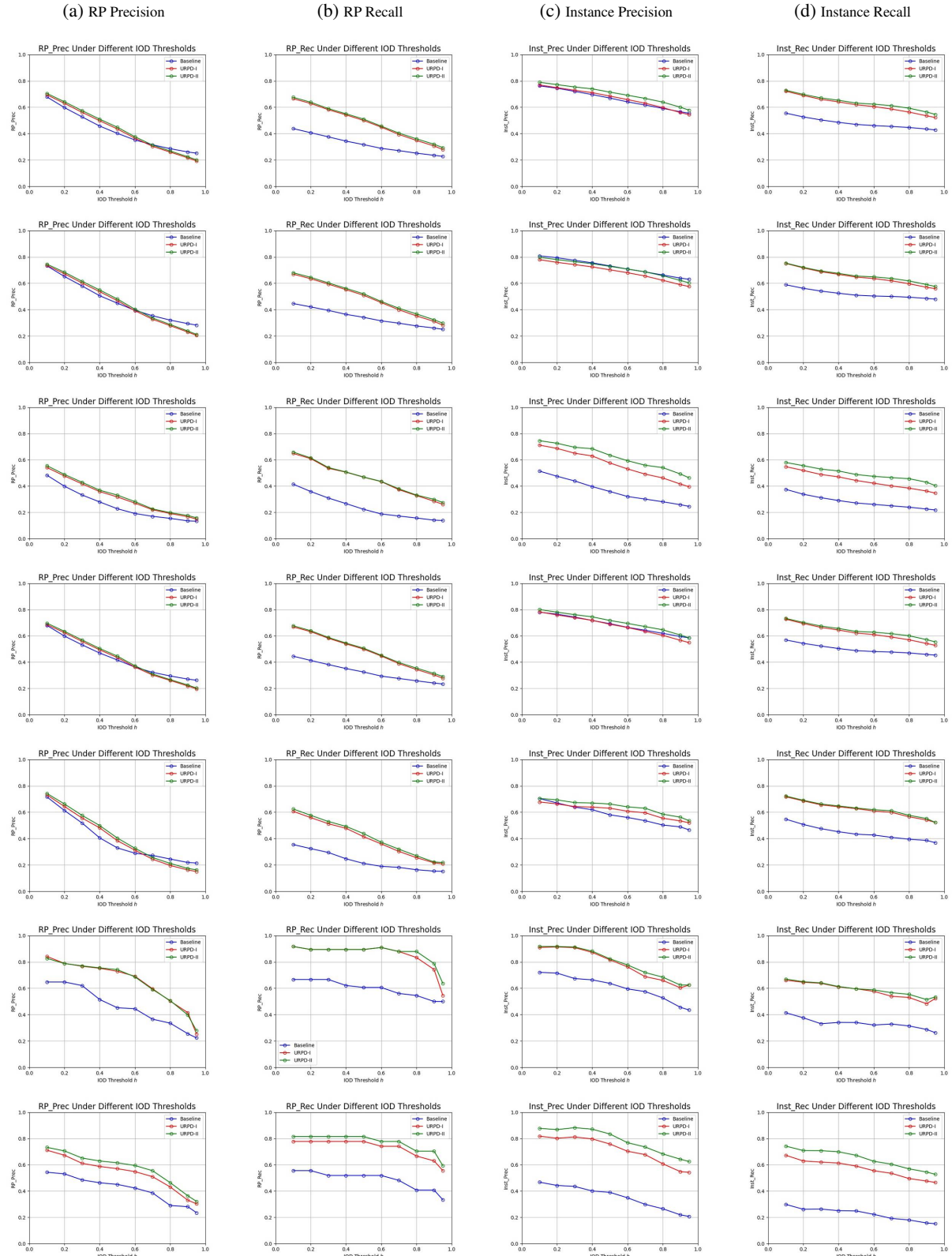


Figure 22: IOD Curves showing each evaluation metric at different IOD thresholds h . **Blue:** the **baseline method**[5]. **Red:** ours **RESCU-I**. **Green:** ours **RESCU-II**. **Top Row:** Full **RP-1K** dataset. **Second Row to Bottom Row:** Results broken out by subset categories: Front View, Projective View, Man-Made Rigid, Man-Made Deformable, Painting, Animal/Human subsets. **Row 3, 6 (b):** the baseline [5] cannot detect the same RP as RESCU does.

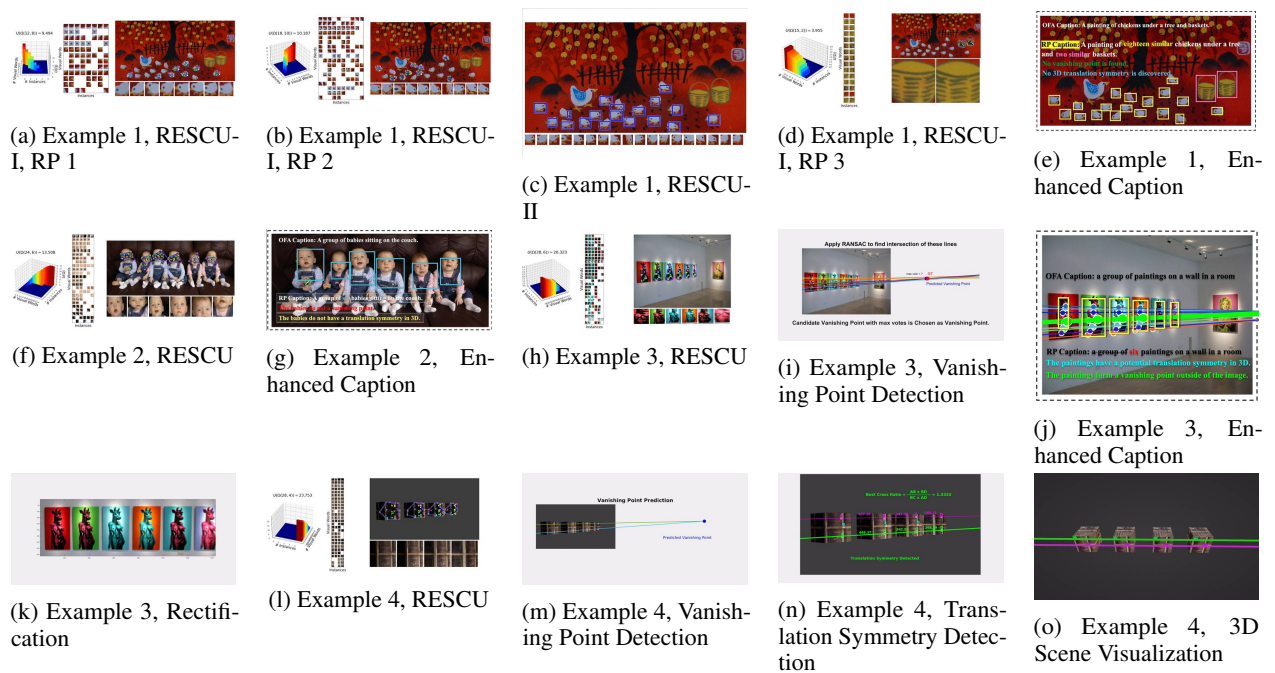


Figure 23: Demo video representative frames